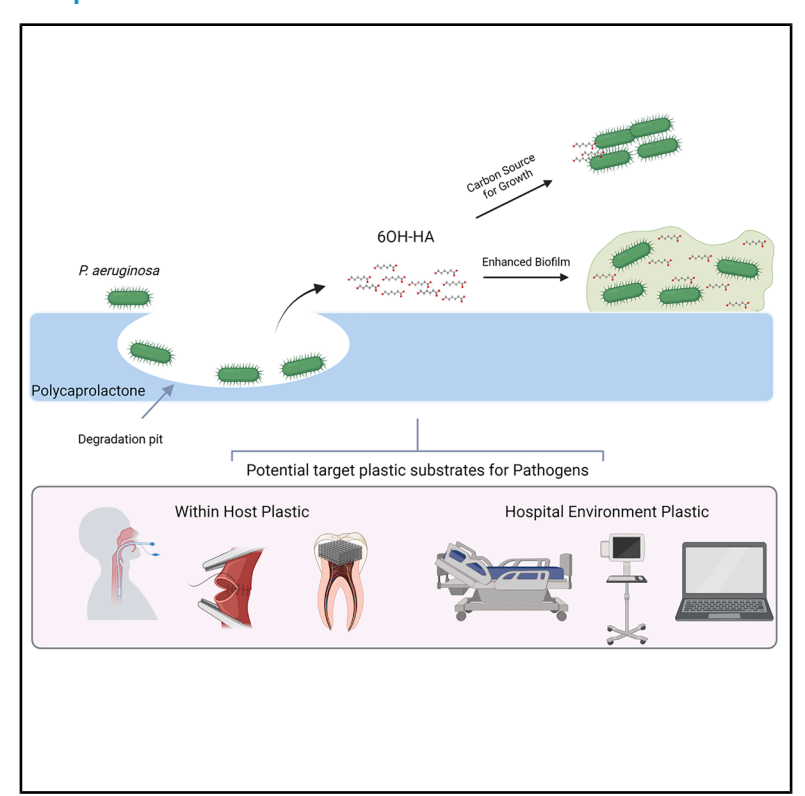
# Pseudomonas aeruginosa clinical isolates can encode plastic-degrading enzymes that allow survival on plastic and augment biofilm formation

#### **Graphical abstract**



#### **Authors**

Sophie A. Howard, Rubén de Dios, Evgenia Maslova, Antonis Myridakis, Thomas H. Miller, Ronan R. McCarthy

#### Correspondence

ronan.mccarthy@brunel.ac.uk

#### In brief

Howard et al. demonstrate that clinical isolates of the opportunistic pathogen *Pseudomonas aeruginosa* can encode functional plastic-degrading enzymes and that these enzymes can influence bacterial biofilm formation.

#### **Highlights**

- Clinical isolate of Pseudomonas aeruginosa PA-W23 can degrade a medically relevant plastic
- Encodes novel polyesterase Pap1, which is responsible for plastic-degrading activity
- P. aeruginosa PA-W23 can use plastic as a carbon source to grow
- Pap1 can influence virulence phenotypes, such as biofilm formation, in the presence of plastic







#### **Article**

# Pseudomonas aeruginosa clinical isolates can encode plastic-degrading enzymes that allow survival on plastic and augment biofilm formation

Sophie A. Howard, <sup>1,3</sup> Rubén de Dios, <sup>1,3</sup> Evgenia Maslova, <sup>1</sup> Antonis Myridakis, <sup>2</sup> Thomas H. Miller, <sup>1,2</sup> and Ronan R. McCarthy <sup>1,4</sup>, \*

<sup>1</sup>Centre for Antimicrobial Innovations, Division of Biosciences, Department of Life Sciences, College of Health and Life Sciences, Brunel University of London, UB8 3PH Uxbridge, UK

<sup>2</sup>Centre for Pollution Research and Policy, Division of Environmental Sciences, Department of Life Sciences, College of Health and Life Sciences, Brunel University of London, UB8 3PH Uxbridge, UK

<sup>3</sup>These authors contributed equally

#### **SUMMARY**

Multiple bacteria encoding plastic-degrading enzymes have been isolated from the environment. Given the widespread use of plastic in healthcare, we hypothesized that bacterial clinical isolates may also degrade plastic. This could render plastic-containing medical devices susceptible to degradation and failure and potentially offer these pathogens a growth-sustaining substrate, enabling them to persist in the hospital-built environment. Here, we mined the genomes of prevalent pathogens and identified several species encoding enzymes with homology to known plastic-degrading enzymes. We identify a clinical isolate of *Pseudomonas aeruginosa* that encodes an enzyme that enables it to degrade a medically relevant plastic, polycaprolactone (PCL), by 78% in 7 days. Furthermore, this degradation enables the bacterium to utilize PCL as its sole carbon source. We also demonstrate that encoding plastic-degrading enzymes can enhance biofilm formation and pathogenicity. Given the central role of plastic in healthcare, screening nosocomial bacteria for plastic-degrading capacity should be an important future consideration.

#### INTRODUCTION

In healthcare settings, plastic is widely used in furniture, single-use medical equipment, and medical implants. <sup>1,2</sup> Plastic medical implantable devices include catheters and ventilator endotracheal tubing, which are commonly made from polyvinyl chloride (PVC), and pacemakers, which contain polyurethane (PU); various vascular implants can be made from polyethylene terephthalate (PET); and surgical mesh and sutures are commonly made from polypropylene (PP) and biodegradable polycaprolactone (PCL). <sup>2–5</sup> All these plastic medical implants are at risk of being an infection site. <sup>6–11</sup> These tend to result from contamination during implantation, followed by the formation of bacterial biofilms on the plastic, leading to difficult-to-treat infections.

Among the plastics used in direct medical applications, the synthetic polyester PCL is becoming increasingly prevalent as it is biodegradable, biocompatible, and bioresorbable. It has had a well-established and important role in medicine since the 1950s, with a variety of medical uses, such as in sutures, <sup>12–15</sup> as a composite for dental fillings, <sup>16,17</sup> and as a collagen-stimulator dermal filler. <sup>18–20</sup> It is generally preferred to other plastic polymers because it has better viscoelastic properties, a low melting temperature, high biocompatibility, and can be mixed

with copolymers or three-dimensional (3D) printed.<sup>21–23</sup> For these reasons, it is also used extensively in wound dressings and healing applications, as it can be loaded with therapeutic drugs, such as antimicrobials or healing-promoting compounds.<sup>24–26</sup> This has led to its successful implementation as a substrate for drug delivery applications.<sup>27–30</sup> Furthermore, part of the growing popularity of this plastic is attributed to its use in tissue engineering applications, including bone scaffolds, highlighting its increasingly prominent role at the forefront of innovative medical interventions.<sup>23,31–34</sup>

It is widely recognized that some environmental bacteria have developed the capacity to degrade different types of plastic, including the aforementioned PET and PCL, by utilizing existing enzymes capable of breaking down structurally similar natural polymers, such as cutin.<sup>35</sup> However, this enzymatic potential for plastic degradation has not been explored in clinically relevant bacteria. Bacterial colonization of catheters, ventilators, and implants and the associated infections are already a major concern in hospitals. However, degradation of a medical implant by a pathogen would compromise the integrity of these implants or create deeper niches for colonization, significantly complicating the treatment of the potential infection. Furthermore, there would also be the possibility that a plastic-degrading pathogen



<sup>&</sup>lt;sup>4</sup>Lead contact

<sup>\*</sup>Correspondence: ronan.mccarthy@brunel.ac.uk https://doi.org/10.1016/j.celrep.2025.115650



could use the plastic as a carbon source to facilitate its growth, thus potentially worsening the colonization and infection of the host. This could also mean that pathogens with the capacity to degrade plastic could persist on plastic surfaces in the hospital for prolonged periods using the plastic as a carbon source. A further concern is that many plastics also contain harmful chemicals, which may cause complications if leached into the host. <sup>36</sup>

Here, we performed a genomic screening of human pathogens to search for potential homologs to known plastic-degrading genes. We identified a novel PCL-degrading enzyme in a wound isolate of *Pseudomonas aeruginosa* and found that the presence of PCL drives a significant increase in biofilm formation, an important virulence factor linked to the routine failure of frontline therapeutics, and can increase *in vivo* virulence.

#### **RESULTS**

## Genome mining identifies polyesterase homologs in human pathogen clinical isolates

To screen clinical isolates for potential plastic-degrading enzymes, we searched pathogenic species (Table S1) for homologs to 23 functional and previously characterized polyesterdegrading enzymes derived from PAZY.eu (Table S2). We found 871 total hits through Protein BLAST for the 23 known enzymes. From these hits, those with a clinically relevant isolation source (blood, wound, etc.) were selected as true clinical hits (a total of 94 unique proteins across 15 pathogenic species). A condensed hit table including the 40 proteins with both query cover and percent identity above 35% is shown in Table S3 (an expanded hit table can be seen in Table S4). These proteins, which come from a variety of pathogens (e.g., Streptococcus pneumoniae, P. aeruginosa, Enterobacter ludwigii, Leclercia adecarboxylata [Enterobacteriaceae], Klebsiella pneumoniae, Enterobacter cloacae, Acinetobacter baumannii, and Mycobacterium tuberculosis), are more likely to share function with known polyester-degrading enzymes based on active site conservation. Among them, two carboxylesterase type B proteins (GenBank: CJS43715.1 and COC83087.1) from S. pneumoniae strains isolated from nasopharynx samples in Thailand showed an identity >60% (100% query cover and 98.57% identity and 98% query cover and 63.71% identity to the known functional polyesterase BsEstB, respectively). An alpha/beta hydrolase (GenBank: RPM52859.1) from a P. aeruginosa wound isolate from the United Kingdom also had a sequence identity above the 60% threshold.37 This enzyme had 87% query cover and 61.76% identity to the previously characterized polyester-degrading enzyme PET5.38 A phylogenetic tree of all the hits and known polyester-degrading enzymes shows their close evolutionary relationships (Figure 1). Overall, this analysis suggests that the enzymatic potential to degrade plastic is encoded within the genomes of a diverse array of clinically relevant pathogens.

Among the hits with a sequence identity greater than 60%, we selected the alpha/beta hydrolase RPM52859.1, which is evolutionarily related to many of the known functional plastic-degrading enzymes, to be expressed in an *Escherichia coli* host and test it for plastic-degrading activity. Critically, we were also able to

obtain the source clinical isolate, *P. aeruginosa* PA-W23, allowing further characterization of the impact of plastic-degrading properties on this pathogen's behavior.

Due to the clinical origin of RPM52859.1 (P. aeruginosa PA-W23, isolated from a wound), we named this protein Pap1, for pathogen-associated polyesterase 1. Pap1 did not show a predicted conventional signal peptide (SP) according to SignalP (probability: 0.018). However, SecretomeP, an algorithm to detect non-conventional secreted proteins, indicated that Pap1 was secreted (score: 0.933978; a score of >0.5 indicates possible secretion). The closest BLASTp match, PET5, does contain a traditional SEC (general secretion pathway) SP detectable with SignalP (probability: 0.603), so we compared Pap1 to PET5, removing the SP of the latter. The N termini still had a low identity, but overall, an alignment using EMBOSS Needle showed that the two proteins had 58.4% identity and 73.7% similarity (Figure 2A). Pap1 is classified as a type IIa PETase-like enzyme, with the exception that one residue of sub-site I (tyrosine-172) does not meet the consensus of the known types, which harbor a tryptophan.<sup>39</sup> Additionally, it has a dienelactone hydrolase domain (residues 58-224), which is found in several other polyester-degrading enzymes. 40-42 Although PET5 was the best genomic match for Pap1, the structure of PET5 has not been solved. A Phyre2 prediction of Pap1 (Figure 2B) had a top structural match to PET2 (PDB: 7EC8).43 Except for the N-terminal regions, the superposition of the Pap1 and PET2 protein structures yielded a good alignment, including with the catalytic triad (Figure 2C), quantified with a root-mean-square deviation (RMSD) of 0.179 Å (where an RMSD of <2 Å is considered a good alignment). Additionally, alignment with the commonly studied and well-characterized IsPETase (PDB: 5XJH), another polyester-degrading enzyme, gave an RMSD of 1.21 Å (Figure S1).39 A BLASTp search of Pap1 restricted to P. aeruginosa species provided one high-similarity match, WP\_201266253.1 (99.58% identity and 84% query cover to Pap1) from an unknown isolation source. Without species restriction, Protein BLAST finds more high similarity matches in Stutzerimonas stutzeri (previously Pseudomonas stutzeri; 100% guery cover and 91.1%-98.9% identity). This species is widely distributed in the environment but is considered an opportunistic pathogen.44 The top 100 BLASTp hits to Pap1, which include PET5 and PET2, are shown in the phylogenetic tree included in Figure S2. Pap1's structural similarity to the known functional polyesterases and conservation of polyesterdegrading sites were promising indicators of the functionality of Pap1.

#### Pap1 is a functional PCL-degrading enzyme

Several species of *Pseudomonas* are known to encode promiscuous lipases and esterases that can act on PCL, <sup>45</sup> but thus far, no clinical isolate of *P. aeruginosa* has been identified with this activity. A pathogen encoding enzymes with putative plastic-degrading activity does not necessarily mean these enzymes are functional or have PCL-degrading activity. To assess if Pap1 was functional and capable of degrading PCL, we synthesized and cloned the *pap1* gene from *P. aeruginosa* PA-W23 into the expression vector pET20b in frame with the vector-encoded *pelB* SEC secretion SP and subsequently transformed it into

#### **Article**



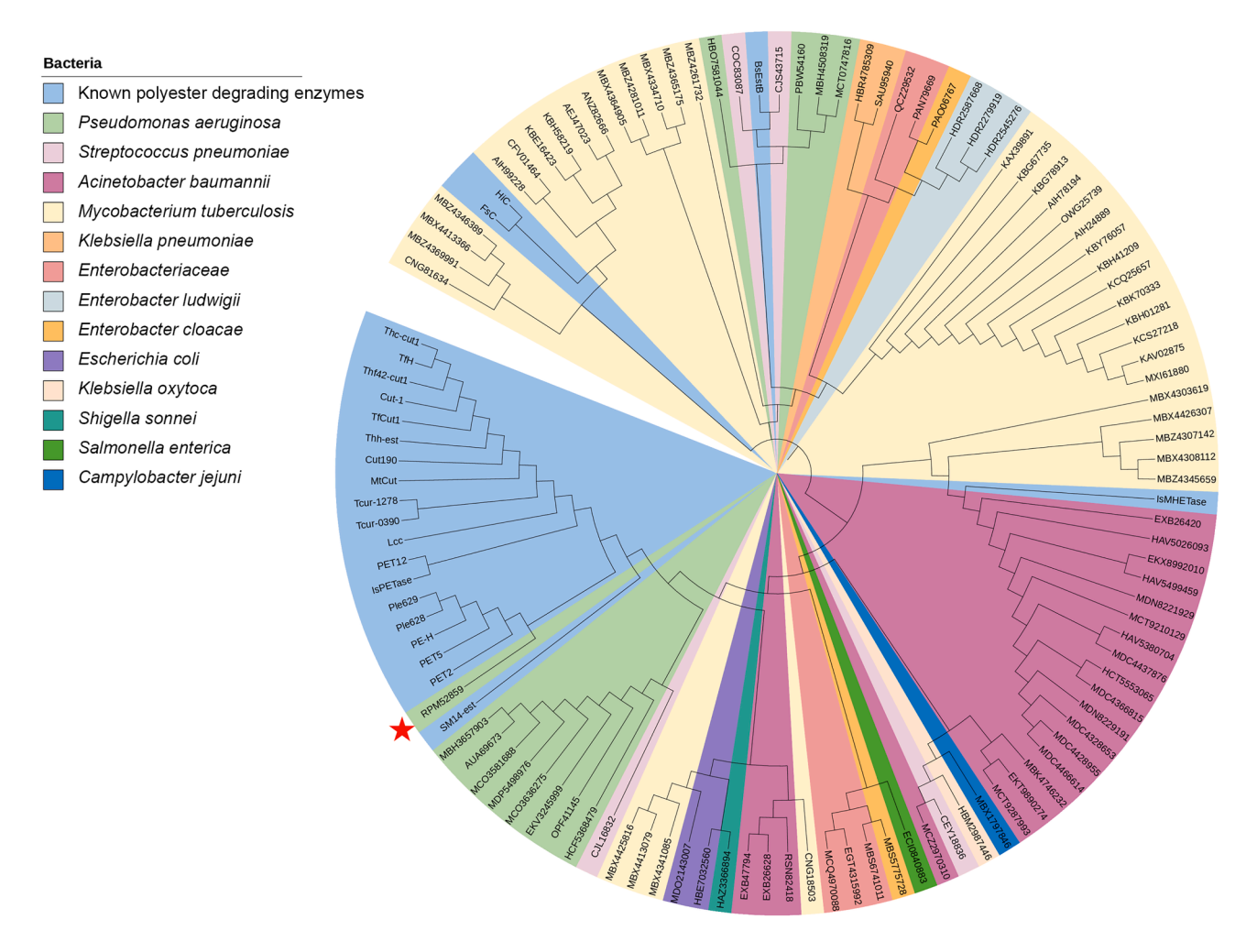


Figure 1. Phylogenetic tree analysis of clinically relevant BLAST protein hits

A neighbor-joining tree was constructed using the *p* distance of the protein sequences. Hits are color coded by bacteria. Pap1 is indicated by a star.

an *E. coli* BL21 Star (DE3) pLysS host strain. To test the Pap1 functionality, the *E. coli* host carrying pET20b-*pap1\_SP* was spotted on PCL-agar plates. PCL was chosen because of its medical relevance, its use as a model polyester-degrading substrate for microbiological analysis, and its amenability to a range of qualitative and quantitative assays to determine polyesterase activity. <sup>42</sup> Inducing *pap1* expression with 0.5 mM IPTG resulted in a clear zone of PCL degradation, confirming it is indeed a functional polyesterase (Figures 2D and 2F). As expected, a control *E. coli* host carrying the empty pET20b plasmid resulted in no PCL degradation (Figures 2E and 2F).

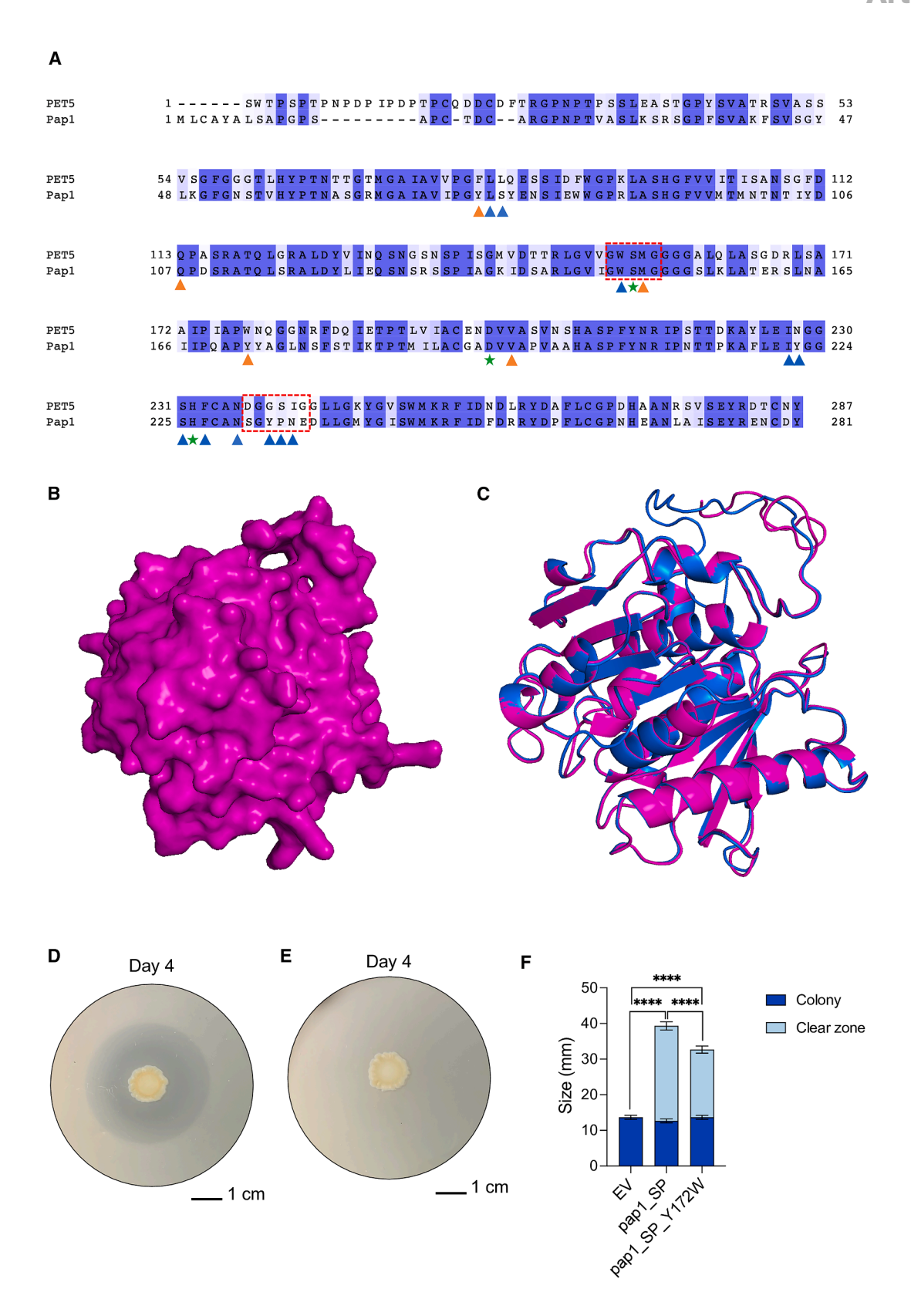
Pap1 is classified as a type IIa PETase-like enzyme except for a change in the sub-site I conserved tryptophan to tyrosine (Y172). To assess the relevance of this amino acid substitution for the enzymatic activity, we tested its effect by producing a Pap1 variant with a Y172W residue change in the aforementioned *E. coli* host and comparing it to the original Pap1 in a PCL degradation assay. This sequence change resulted in a significantly decreased PCL degradation, highlighting the importance of this non-consensus amino acid for the activity of Pap1

(Figure 2F). Altogether, these results confirm the activity of Pap1 as a functional PCL-degrading enzyme.

## The Pap1 native clinical isolate degrades PCL and can use it as a carbon source

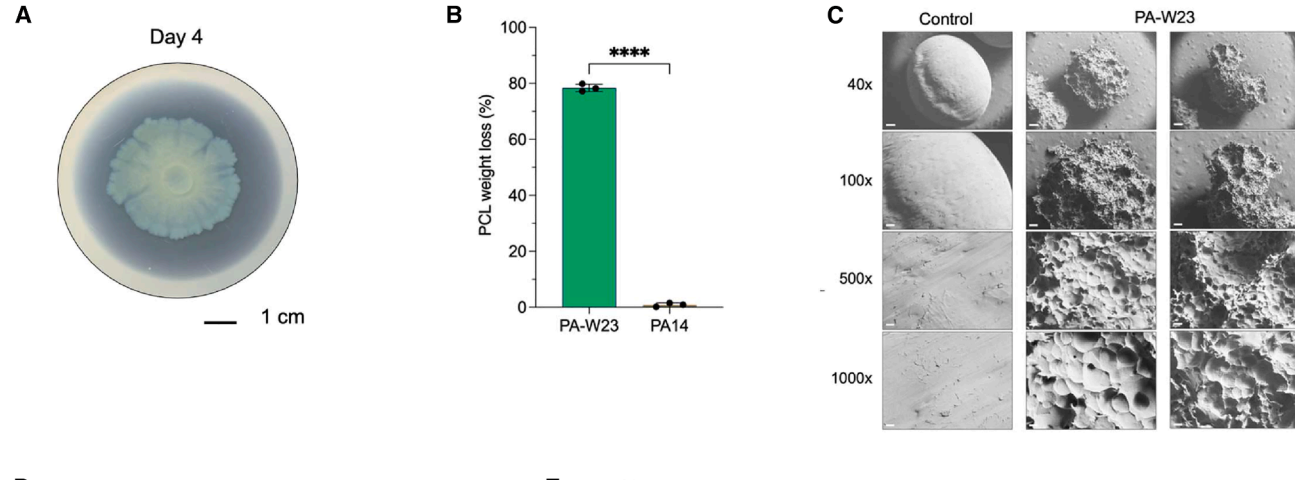
At this point, we demonstrated that Pap1 is functional when heterologously expressed in an *E. coli* host. However, we wanted to elucidate the functionality of this enzyme in its native pathogenic host. To assess this, we obtained the original pap1-encoding clinical isolate, *P. aeruginosa* PA-W23, and tested its PCL-degrading activity. We initially confirmed its PCL-degrading activity on PCL agar (Figure 3A), with the zone appearing clearer than when pap1 is expressed in *E. coli* (Figure 2D). This revealed that the *P. aeruginosa* PA-W23 clinical isolate is capable of PCL degradation. To obtain a greater resolution of the PCL degradation by this clinical strain, we subsequently quantified PCL weight loss by PA-W23 in rich media (LB, Luria-Bertani), obtaining 78.4% PCL weight loss in 7 days (Figure 3B). As a control, the non-PCL-degrading *P. aeruginosa* strain PA14 did not produce any notable PCL weight loss in the same conditions. Scanning electron microscopy (SEM)





#### **Article**





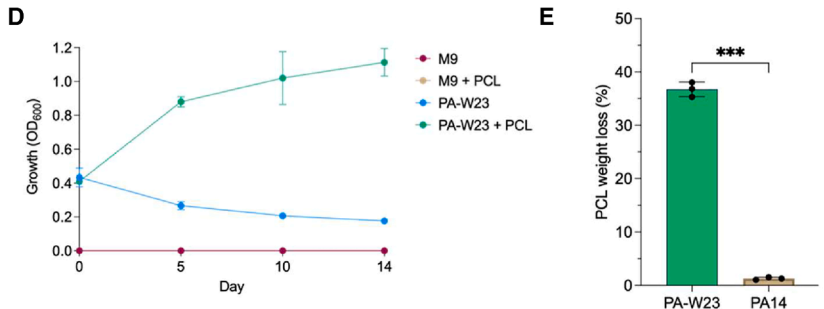


Figure 3. PCL degradation and use as sole carbon source by P. aeruginosa PA-W23

(A) P. aeruginosa PA-W23 spotted onto PCL agar plates, representative photograph of day 4; scale bar: 1 cm.

(B) Weight loss assay of PCL in LB after a 7-day incubation with PA-W23 and PA14. Weight loss is normalized to an uninoculated control. Mean and SD of 3 repeats; statistical analysis using a parametric t test with Welch's correction; \*\*\*\*p < 0.0001.

(C) Representative SEM images of 3 PCL beads each from 7-day weight loss assays in LB, control LB (left), and PA-W23 incubation (middle and right). First row:  $40 \times$  magnification (scale bar:  $400 \mu$ m); second row:  $100 \times$  magnification (scale bar:  $400 \mu$ m); third row:  $500 \times$  magnification (scale bar:  $400 \mu$ m); and fourth row:  $1,000 \times$  magnification (scale bar:  $200 \mu$ m).

(D) Growth curve in M9 minimal media over 14 days with PCL as the sole carbon source; mean and SD of 3 repeats.

(E) Weight loss of PCL beads after 14-day incubation in M9 minimal media with PA-W23 and PA14. Weight loss is normalized to an uninoculated control. Mean and SD of 3 repeats; statistical analysis using a parametric t test with Welch's correction; \*\*\*p < 0.001.

analysis of the PCL beads exposed to PA-W23 showed deep pits and cavities in the surface, as well as an overall reduced size of the bead (Figure 3C). This level of PCL degradation by a clinical isolate highlights how the structural integrity of any PCL-containing medical device, such as sutures or implants, could be severely compromised by a pathogen with the capacity to degrade it. Next, we wanted to assess whether PA-W23 could not only degrade PCL but also metabolize it. For this, we performed a

growth curve assay in M9 minimal media with PCL beads as the only possible carbon source, using M9 minimal media with no carbon source as a control. The results confirmed that PA-W23 can indeed use PCL as a sole carbon source (Figure 3D). We also assessed PCL weight loss in M9 minimal media over 14 days and demonstrated a 36.73% reduction in PCL weight, whereas there was negligible weight loss in a control inoculated with PA14 (Figure 3E). Being able to utilize plastic as a carbon source may

#### Figure 2. P. aeruginosa clinical isolate PA-W23 possesses a polyesterase homolog

(A) Protein sequence alignment of Pap1 and PET5, percent identity colored in Jalview set to 30% conservation. Annotation: the red box is the Gly-x1-Ser-x2-Gly motif, orange triangles demarcate sub-site I, blue triangles demarcate sub-site II, and green stars demarcate the catalytic triad. The signal peptide was removed from PET5.

(B) Phyre2-predicted structure of Pap1, surface shown, 95% of residues modeled with >90% confidence, catalytic triad colored in green.

(C) Phyre2-predicted structure of Pap1 aligned with PET2 (PDB: 7EC8) using PyMOL command cealign, resulting in RMSD of 0.179 (Å) over 256 residues. The PET2 structure is shown in blue, the Pap1-predicted structure is shown in magenta.

(D) E. coli BL21 Star (DE3) pLysS expressing Pap1\_SP spotted onto PCL agar plates, representative photograph of day 4 out of 3 biological replicates; scale bar: 1 cm. Agar plates contain 1% PCL and 0.5 mM IPTG for enzyme induction.

(E) BL21 Star (DE3) pLysS carrying empty pET20b spotted onto PCL agar plates, representative photograph of day 4 out of 3 biological replicates; scale bar: 1 cm. (F) PCL clear zone assay after 4 days testing empty vector (EV), Pap1\_SP and Pap1\_SP\_Y172W expressed in *E. coli* BL21 Star (DE3) pLysS; mean and standard deviation (SD) of 3 repeats. Statistical analysis was performed by two-way ANOVA with Tukey's correction \*\*\*\*p < 0.0001.



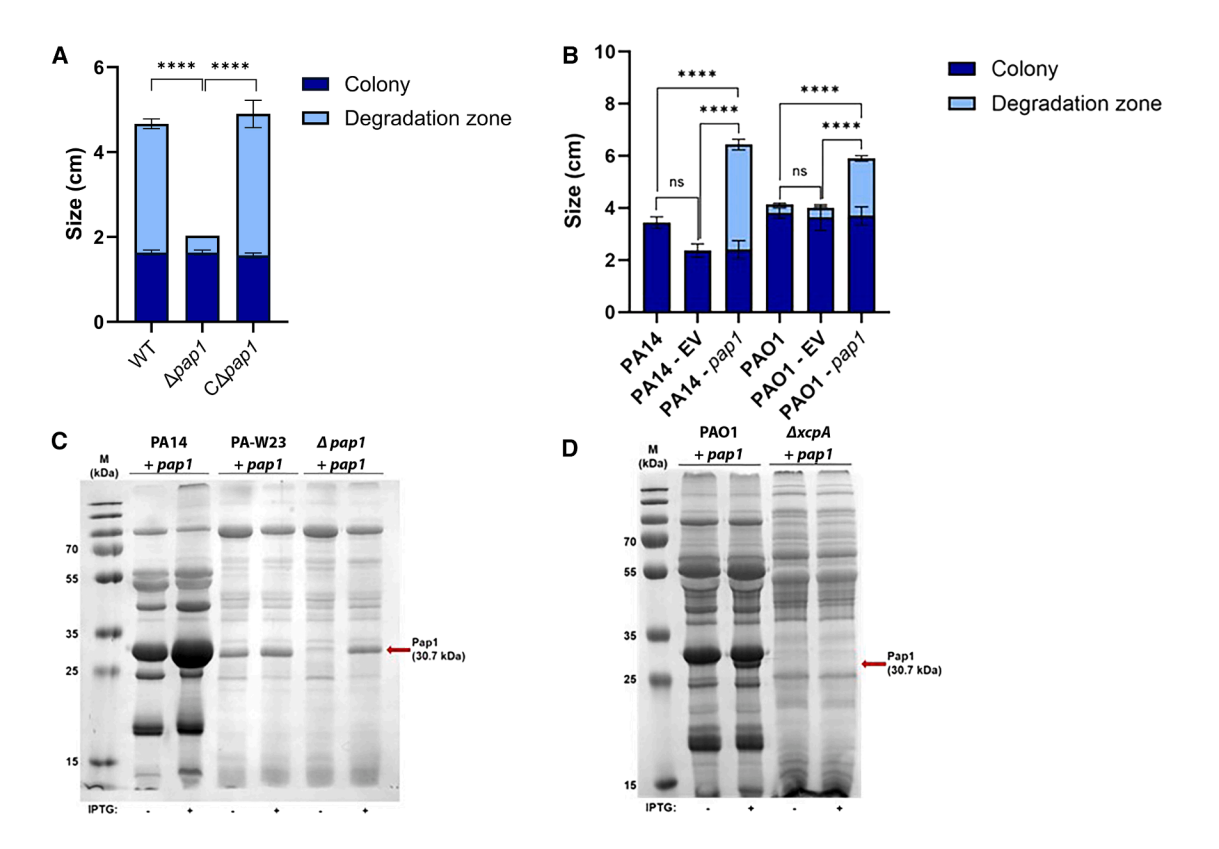


Figure 4. P. aeruginosa PA-W23 degrades PCL using Pap1

(A) PCL clear zone assay after 4 days testing *P. aeruginosa* PA-W23, its derivative Δ*pap1* mutant, and the complemented mutant (Δ*pap1* with *pap1*\_noSP expressed from miniTn7 transposon); mean and SD of 3 repeats are represented; \*\*\*\*\*p < 0.0001. Empty vector (EV) controls can be seen in Figure S4.

(B) PCL clear zone assay after 4 days testing PA14 WT, WT with EV, and overexpressor (WT with Pap1\_noSP) and PA01 WT, WT with EV, and overexpressor (WT with Pap1\_noSP); mean and SD of 3 biological replicates are represented. Statistical analysis was done by two-way ANOVA with Tukey's correction.

\*\*\*\*\*p < 0.0001: ns. non-significant.

(C) SDS-PAGE gel image of secreted protein fractions from *P. aeruginosa* PA14, PA-W23, and the complemented Δ*pap1* mutant, all carrying a miniTn7 insertion to induce the expression of *pap1* with the *lacl<sup>q</sup>-Ptac* system. The secreted protein fractions were obtained from cell-free culture supernatants of these strains after growing in the presence or absence of 1 mM IPTG for 18 h (as detailed in the STAR Methods). The red arrow indicates the band corresponding to Pap1 (theoretical molecular weight of 30.7 kDa). One representative image out of 3 biological replicates is shown.

(D) SDS-PAGE gel image of secreted protein fractions from *P. aeruginosa* PAO1 and its mutant derivative ΔxcpA (T2SS defective), both carrying a miniTn7 insertion to induce the expression of pap1 with the lacl<sup>q</sup>-Ptac system. The secreted protein fractions were obtained from cell-free culture supernatants of these strains after growing in the presence or absence of IPTG 1 mM for 18 h (as detailed in the STAR Methods). The red arrow indicates the band corresponding to Pap1. One representative image out of 3 biological replicates is shown.

enable pathogens to persist within the host or the hospital-built environment for prolonged periods under nutrient-limiting conditions. Interestingly, the rate of degradation was more than double in rich media as compared to minimal media, which suggests that even in optimal growth and carbon non-limiting conditions, *pap1* is still expressed.

#### Pap1 is secreted via the type II secretion system

To conclusively assign the polyester-degrading activity of PA-W23 to Pap1, we constructed a  $\Delta pap1$  deletion mutant. This mutation did not produce a growth defect (Figure S3). A PCL degradation assay comparing the  $\Delta pap1$  mutant to the parental strain resulted in the almost complete loss of the PCL-degrading activity in the absence of this enzyme and its recovery after chromosomal complementation (Figure 4A). We also overexpressed pap1 in the wild-type (WT) PA-W23 background, and although a significant increase in PCL degradation was observed, the increase was rela-

tively small (Figure S5), suggesting that *pap1* was already being expressed at high levels within the cell and Pap1 secretion is the bottleneck for its activity. In comparison, introducing *pap1* into a neutral site in the chromosome of the non-plastic-degrading clinical isolate *P. aeruginosa* PA14 and the lab strain *P. aeruginosa* PA01 conferred significant levels of PCL-degrading activity (Figure 4B). 46 This confirmed that the PCL-degrading activity provided by Pap1 can be transferred to other hosts.

As a next step, we wanted to confirm that Pap1 was secreted to the media, as was suggested by our previous results. To do this, we grew cultures of PA-W23, its  $\Delta pap1$  derivative, and the non-degrading strain PA14 expressing pap1 from a neutral-site miniTn7 transposon insertion, as well as their respective empty vector controls. Cell-free supernatant of these cultures was spotted on PCL agar, showing that supernatant from the strains expressing pap1 produced a clear degradation zone after only 6 h, as opposed to the control strains lacking pap1 (Figure S5).

#### **Article**



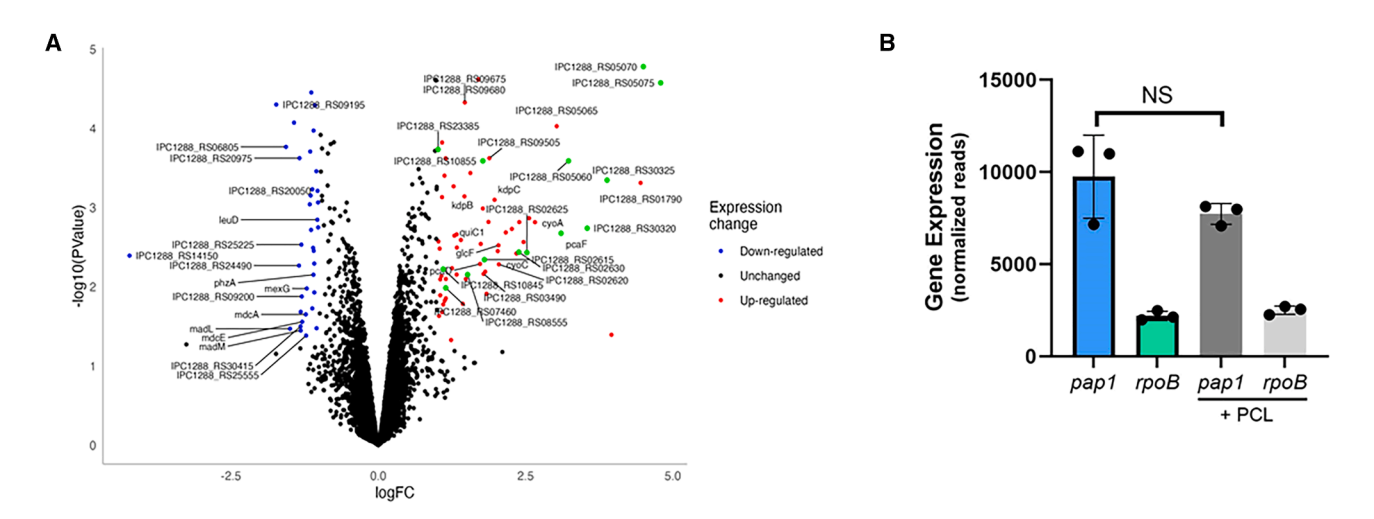


Figure 5. Transcriptional response to PCL exposure

(A) Volcano plot representing dRNA-seq results from comparing global transcription in the presence of PCL in starvation media (10% LB). According to the dRNA-seq results, 65 genes were upregulated (red) and 36 were downregulated (blue) more than 1 logFC in the presence of PCL. Genes linked to fatty acid metabolism are highlighted in green.

(B) Expression of pap1 in the presence and absence of PCL. Comparison of constitutively expressed housekeeping gene rpoB also shown. ns, non-significant.

This clearly indicates that the Pap1 enzyme is secreted to the media. To further confirm this, we harvested, precipitated, and resuspended the protein content of supernatants from PA14, PA-W23. and its  $\Delta pap1$  derivative bearing the pap1-expressing miniTn7 insertion, in which IPTG was added to induce pap1 expression along with the respective non-induced controls. SDS-PAGE of these secreted protein fractions demonstrated that a band corresponding to Pap1 (theoretical molecular weight: 30.7 kDa) appeared in the PA-W23 samples but not in the non-induced complemented  $\Delta pap1$  mutant sample, with the band reappearing in the complemented mutant upon IPTG induction (Figure 4C). This conclusively shows that Pap1 is a secreted PCL-degrading enzyme. In the case of PA14, an abundant protein band of similar size to Pap1 and specific to this strain made it difficult to distinguish the Pap1 band, although it is clear that the intensity of the band increases in the IPTG-induced PA14 sample.

To obtain further insights into the mechanism through which Pap1 is translocated to the extracellular milieu, we decided to identify the secretion system involved in this process. In P. aeruginosa, proteins are typically secreted via four general systems: type 1 secretion system (T1SS), T2SS, T3SS, and T5SS. Taking advantage of the conserved secretion mechanism of Pap1, we decided to test this in strain PAO1, for which mutant derivatives in key genes of each secretion system were available (except for T1SS). We selected mutants in essential genes of each secretion system, including  $\Delta xcpA$  (T2SS), ΔpscN (T3SS), and ΔtpsB4 (T5SS),46 and introduced the pap1-encoding miniTn7 transposon in them as well as in the WT PAO1, along with an empty vector control. As explained above, we tested the PCL-degrading activity of cell-free supernatants obtained after growing those strains in the presence of IPTG. This experiment revealed that only the AxcpA mutant (T2SS defective) could not produce a degradation zone, whereas the  $\Delta pscN$  and  $\Delta tpsB4$  mutants produced degradation zones similar to that of the WT PAO1 (Figure S6). Further supernatant protein precipitation and SDS-PAGE assays demonstrated that Pap1 cannot be recovered from the secreted fraction when expressed in the  $\Delta xcpA$  mutant background (Figure 4D). Altogether, these results demonstrate that Pap1 secretion is mediated by the T2SS.

## P. aeruginosa PA-W23 uses PCL via fatty acid metabolism

To better understand how PA-W23 responds to the presence of PCL, we performed a differential RNA sequencing (dRNA-seq) analysis in the presence and absence of PCL. PA-W23 cultures were grown in starvation media (10% LB ± PCL) until the midexponential phase. This medium was selected to maximize the effect of degrading PCL on global transcription while sustaining a certain level of growth in the absence of PCL and preventing any derived transcriptional noise due to stress. Within the resulting transcriptional dataset, there were 101 differentially regulated genes (log fold change [logFC] > 1) (Figure 5A; Table S5). Several of the genes that were significantly upregulated were associated with fatty acid metabolism. The fatty acid 6OH-hexanoic acid (6OH-HA) is the degradation product of PCL. This suggests that the accumulation of this fatty acid via PCL depolymerization would facilitate growth in nutrientlimiting conditions by supplying metabolites that can eventually be fed into the Krebs cycle, as demonstrated in our results above, which show that PA-W23 can use PCL as a sole carbon source. Interestingly, pap1 was not among the significantly differentially expressed genes. This prompted us to investigate the pap1 absolute levels of expression in both conditions tested in the dRNA-seq experiment. Strikingly, pap1 was one of the highest expressed genes in both conditions (Figure 5B), suggesting that pap1 is constitutively expressed to high levels within PA-W23. This is consistent with our previous observation that PA-W23 is able to degrade PCL even when grown in rich media such as LB.





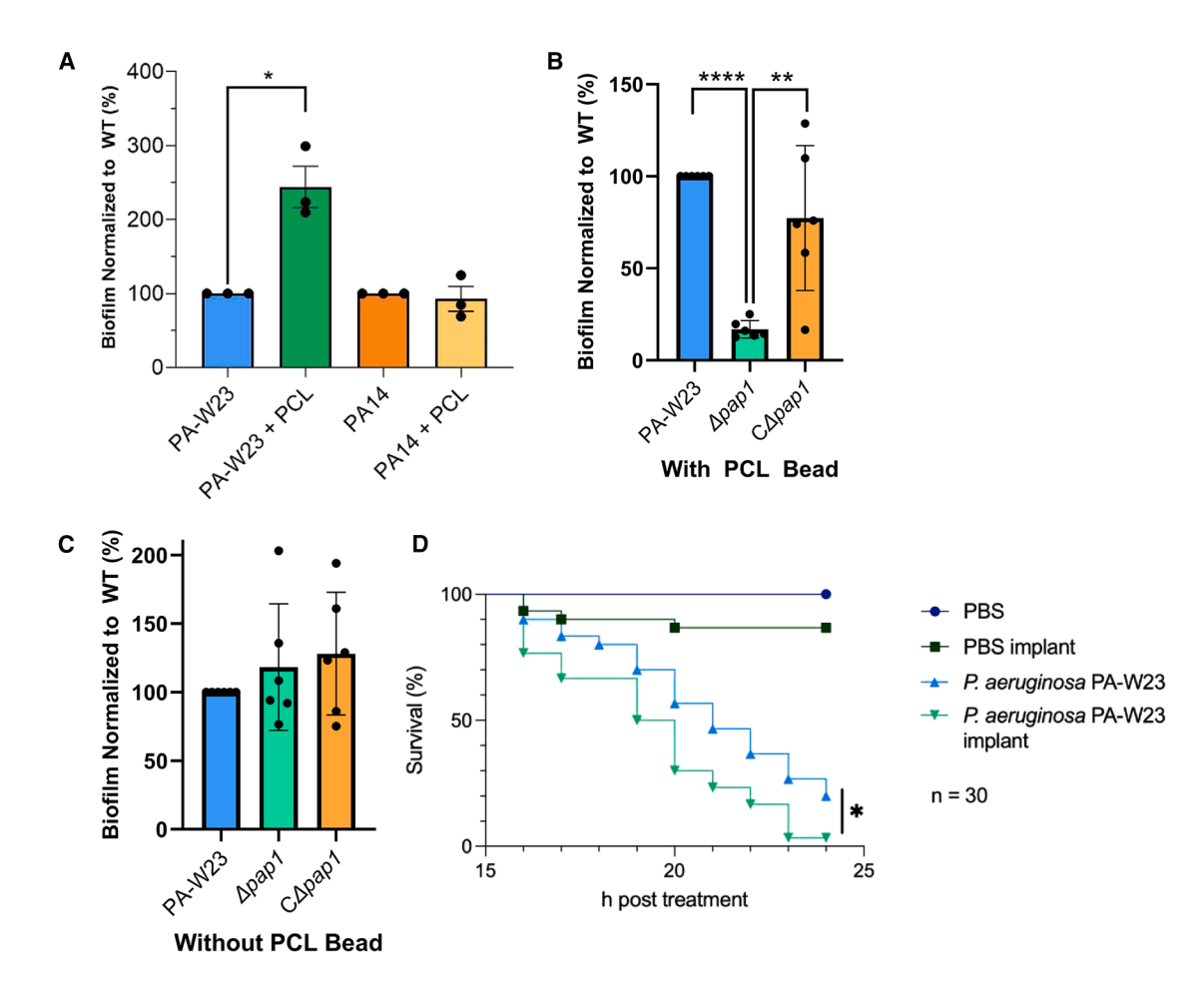


Figure 6. Impact of PCL on P. aeruginosa PA-W23 biofilm and virulence

(A) PA14 and PA-W23 biofilm formation via crystal violet staining with and without PCL bead added to culture. Mean and SD of 3 repeats; statistical analysis using one-way ANOVA with multiple comparisons; \*p < 0.05. Normalized to strain without PCL as 100%.

(B) P. aeruginosa PA-W23 biofilm assay with PCL beads in each well. P. aeruginosa PA-W23  $\Delta pap1$ ,  $\Delta pap1$  with EV, and  $\Delta pap1$  complemented with Pap1\_noSP; mean and SD of three technical replicates and two biological replicates; statistical analysis using one-way ANOVA with multiple comparisons; \*\*p < 0.01; \*\*\*\*p < 0.0001. Normalized to WT as 100%.

(C) *P. aeruginosa* PA-W23 biofilm assay without PCL beads. *P. aeruginosa* PA-W23 Δ*pap1*, Δ*pap1* with EV, and Δ*pap1* complemented with Pap1\_noSP; mean and SD of three technical replicates and two biological replicates; statistical analysis using one-way ANOVA with multiple comparisons resulting in no significant differences. Normalized to WT as 100%.

(D) Survival of *G. mellonella* with and without a PCL implant, injected with either phosphate-buffered saline (PBS) as a control or *P. aeruginosa* PA-W23. Three biological replicates were performed with a minimum of 10 larvae per condition per biological replicate (n = 30). Kaplan-Meier survival curves were used to visualize data, and statistical analysis was performed with a log rank test. \*p < 0.05.

## PCL induces higher biofilm formation and virulence in a PCL-degrading clinical isolate

The capacity to degrade PCL and use it as a carbon source could indirectly boost virulence, expanding the metabolic repertoire of a pathogen and weakening the integrity of PCL-containing medical devices. To explore whether the presence of PCL could directly impact any virulence phenotypes, we measured a key virulence factor in *P. aeruginosa*: biofilm formation. Biofilms are communities of bacteria that are attached to each other or an abiotic/biotic surface. In doing so, they are better protected from the effects of antibiotics and the rigors of the immune system. <sup>47–49</sup> To test the effect of PCL on the biofilm formation of PAW23, we conducted a 96-well plate-based biofilm assay on

strains grown with and without PCL beads (assay setup summarized in Figure S7). This showed that biofilm formation on the surface of the well was significantly higher for PA-W23 when a PCL bead was present (Figure 6A). We chose to measure biofilm on the surface of the well in the 96-well plate rather than on the PCL bead itself since, based on previous data (Figure 3C), the morphology and, as a result, the surface area of the bead are dramatically altered by the PCL-degrading activity of PA-W23. Planktonic PA-W23 colony-forming unit (CFU) counts were not significantly different when grown with and without PCL in the nutrient-rich LB, indicating that this is exclusively a biofilm effect (Figure S8A). To confirm that this increased biofilm was specifically due to the capacity to degrade PCL and not a non-specific

#### **Article**



response to the presence of a plastic bead in the well, we used the non-PCL-degrading strain *P. aeruginosa* PA14 as a control. The presence of PCL had no impact on *P. aeruginosa* PA14 bio-film levels (Figure 6A). To further challenge this hypothesis and rule out that the increased biofilm seen by PA-W23 was a physical response to a bead in each well, we repeated the assay using a non-biodegradable glass bead of similar size. In this assay, the glass bead did not have a significant effect on PA14 biofilm formation and actually resulted in less PA-W23 biofilm formation (Figure S8B), further supporting PCL degradation as the cause of this increase in biofilm formation.

To explore the role of Pap1 in this augmented biofilm phenotype, we assessed the biofilm formation of the *P. aeruginosa* PA-W23 Δ*pap1* mutant and the complemented mutant in the presence of a PCL bead. The loss of *pap1* led to a >85% decrease in biofilm levels, whereas biofilm levels were restored to WT levels upon complementation (Figure 6B). Strikingly, in the absence of the PCL bead, the deletion of *pap1* had no impact on biofilm levels (Figure 6C). This confirms the involvement of Pap1 in the biofilm formation capability of this strain in a plastic-dependent manner and, for the first time, directly links a plastic-degrading enzyme to biofilm levels in its native strain.

Biofilm is intrinsically linked to virulence, so we hypothesized that the impact of PCL on biofilm formation by PA-W23 may impact the overall pathogenic potential of PA-W23. To assess this, we used a previously established *in vivo* implant model in *Galleria mellonella* larvae (Figure S8C).<sup>50</sup> PA-W23 showed an increased virulence in the presence of a PCL implant (Figure 6D) in this assay, therefore suggesting that the ability to degrade and colonize a host-implanted plastic implant by a pathogen would negatively impact the course of an infection. This is further supported by a complementary experiment in which *P. aeruginosa* PA14, which does not degrade PCL, produced similar *G. mellonella* mortality levels regardless of the presence of the implant (Figure S5D). However, the Δ*pap1* mutant did not show significant differences in virulence when comparing the presence and absence of implant (Figure S8E).

## Pap1 degrades PCL into monomers that are directly incorporated into biofilms

To drive such an increase in biofilm formation, it would be expected that the cell would have to upregulate the expression of genes linked to this behavior, such as exopolysaccharide synthesis. However, there were no genes that were directly linked to biofilm formation within the 101 differentially regulated by the presence of PCL. We, thus, hypothesized that there may be a physical interaction between PCL breakdown products and the biofilm matrix, leading to higher biofilm levels. To challenge this hypothesis, we developed a targeted and quantitative liquid chromatography-mass spectrometry (LC-MS) method to measure 60H-HA, the degradation product of PCL. The biofilm biomass was isolated from 96-well plate wells inoculated with PA-W23, PA-W23 Δ*pap1*, or the complemented mutant, which were subsequently incubated with a PCL bead. Analysis of these biofilms revealed that 60H-HA was present in the extracellular matrix at an increased concentration in the case of PA-W23 (46.9  $\pm$  23.3 ng/mL), whereas the 6OH-HA concentration in the biofilm matrix produced by the  $\Delta pap1$  mutant dropped

to 1.2  $\pm$  1.6 ng/mL ( $\sim$ 98% reduction from the WT) (Figures 7A and 7B). The average concentration of the monomer increased to 29.9 ng/mL in the complemented Δpap1 mutant. These measurements agreed with the overall trends produced by PCL in our previous experiments (Figures 6A-6C). The same trend was observed in the analysis of the cell-free supernatant after growth, where 6OH-HA concentrations were reduced by 91% in the supernatant of Δpap1 compared to that of the PA-W23 WT. Importantly, 6OH-HA was measured in the control treatment, which contained only a PCL bead and uninoculated LB broth, at an average concentration of 16,591 ng/mL (Figure 7C). The presence of the monomer in the control was assumed to be the innate leaching of the monomer from the PCL bead. The observed trends in monomer concentrations measured in both the biofilm and supernatant, alongside the increase in biofilm formation, suggest that 6OH-HA is directly incorporated into the biofilm, increasing overall biofilm levels. To further test this hypothesis, we reasoned that the exogenous addition of the 6OH-HA monomer to the media should increase PA-W23 biofilm levels. When assessed, we could observe a significant increase in the PA-W23 biofilm levels (Figure 7D), confirming that the presence of the monomer and its incorporation into the biofilm matrix were sufficient to drive increased levels of biofilm formation in this clinical isolate.

## Enhanced biofilm formation by PCL is conserved in other plastic-degrading *P. aeruginosa* clinical isolates

Up to this point, our screening for plastic-degrading pathogens was entirely in silico. To explore if other non-sequenced clinical isolates of P. aeruginosa had the capacity to degrade plastic, we screened a clinical isolate collection sourced from the British Society for Antimicrobial Chemotherapy Bacteraemia Resistance Surveillance Programme. Among the different P. aeruginosa isolates with varying PCL-degrading properties, we identified one hit that had reproducibly high levels of PCL-degrading activity (Figure S9A). We next sought to explore if this strain had increased biofilm levels similar to what was seen with PA-W23. Strikingly, this strain demonstrated augmented levels of biofilm formation in the presence of a PCL bead as compared to the strain grown without the bead (Figure S9B). This suggests that this mechanism of augmented biofilm formation is conserved among plastic-degrading P. aeruginosa clinical isolates. Future work will now focus on sequencing this plasticdegrading clinical isolate and identifying the enzymes responsible for this activity.

#### **DISCUSSION**

In this work, we have identified a wound clinical isolate of *P. aeruginosa* that can extensively degrade PCL using the novel polyester-degrading enzyme Pap1. We subsequently demonstrate that this capacity to degrade PCL can influence pathogenicity, driving biofilm formation and increasing virulence in the *G. mellonella* model of infection. This poses several clinical challenges with respect to infection. PCL is widely used in medical care and is one of the materials at the forefront of biotechnological innovation due to its favorable biocompatibility profile.<sup>21–23</sup> From a host perspective, the capacity for a pathogen to be



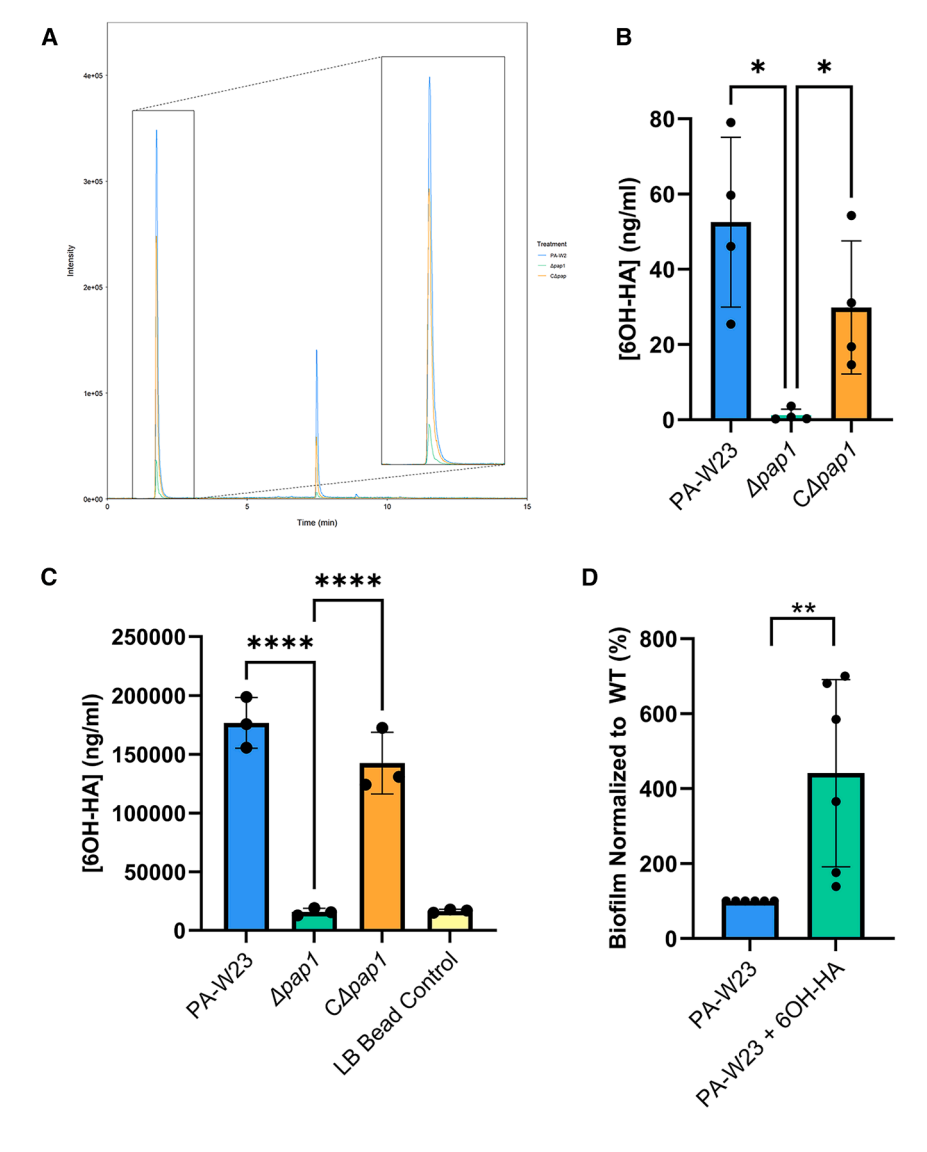


Figure 7. The role of 6OH-HA in PA-W23 biofilm formation

(A) Extracted ion chromatogram of 6OH-HA (quantifier ion) in biofilms isolated from PA-W23 (blue), PA-W23 Δ*pap1* (green), and complemented strain (orange), magnified peak of interest: 1.82 min (inset).

(B) Quantification of 6OH-HA in biofilms isolated from PA-W23, PA-W23  $\Delta pap1$ , and complemented strain. Mean and SD of four biological replicates are represented. Statistical analysis was performed using one-way ANOVA with multiple comparisons; \*p < 0.05.

(C) Quantification of 6OH-HA in supernatant isolated from cultures of PA-W23, PA-W23  $\Delta pap1$ , and complemented strain and uninoculated LB that was incubated with a PCL bead. Mean and SD of three biological replicates are represented. Statistical analysis was performed using one-way ANOVA with multiple comparisons; \*\*\*\*p < 0.0001.

(D) Exogenous supplementation of media with 2.17 mg/mL 6OH-HA enhanced PA-W23 biofilm formation. Mean and SD of six biological replicates are represented; \*\*p < 0.01 with Student's t test.

to the plastic surface and trapped in the biofilm matrix.  $^{42}$  Additionally, high biofilm formation on waste plastics has been linked with better biodegradation in the environment, suggesting this characteristic may also be shared by clinical bacteria that have the capacity to degrade plastic.  $^{58-61}$  Indeed, our findings linking the biofilm formation capabilities of a clinical isolate to its plastic-degrading properties support this hypothesis. To explore the link between biofilm formation and plastic degradation, we assessed the impact of a  $\Delta pap1$  deletion mutant on

the increased biofilm levels seen when PA-W23 is co-incubated with a PCL bead. In this assay, we saw an 85% reduction in biofilm levels compared to the WT strain (Figure 6B). We also confirmed that the addition of PCL as a potential additional carbon source did not impact planktonic cell growth (Figure S3). This indicates that Pap1 is essential in mediating the increased biofilm phenotype. Interestingly, we saw that the  $\Delta pap1$  mutant had comparable levels of biofilm formation to the WT in the absence of the bead (Figure 6C). This highlights the specificity of this response and suggests that the cell is capable of sensing and responding to the presence of PCL within its immediate environment. Transcriptomic analysis uncovered several genes linked to fatty acid metabolism that were upregulated in the presence of PCL, which aligns with the growth assays using PCL as a sole carbon source (Figure 5A). Within the RNA-seq data, however, it was striking that there were no genes directly linked to biofilm formation, as such a dramatic increase in biofilm levels can usually be explained at the transcriptional level by the

able to compromise the structural integrity of any medical device or implant that contains PCL is likely to cause the failure of the medical intervention. From a pathogen perspective, the capacity to degrade this substrate could enable the pathogen to create pits or niches within these devices, shielding the pathogen from the full rigors of the immune system, disinfectants, or antibiotics. The ability of pathogens to use plastic as a carbon source is also a significant concern and could facilitate the persistence of the pathogen within the hospital-built environment or within the host in nutrient-limited conditions.

Biofilms are the dominant mode of growth for bacteria, and adopting this mode of growth can make pathogens particularly recalcitrant to treatment. Biofilm formation is linked to increased tolerance to antimicrobials and immune evasion and is key for chronic infections. Furthermore, our previous work linked this behavior to plastic degradation, as we found that increasing biofilm formation in bacteria boosts plastic degradation and hypothesized that the enzymes are localized

#### **Article**



upregulation of genes associated with biofilm formation, such as polysaccharide biosynthesis machinery and adhesion elements. This prompted us to explore if the increase in biofilm was potentially due to a physical interaction of the biofilm matrix with PCL breakdown products, which would support and enhance the biofilm structure. This theory aligned with a previous report that demonstrated that biofilms can trap plastic nanoparticles within the (exopolysaccharide) EPS matrix.<sup>62</sup> When we assessed the levels of the PCL breakdown product, 60H-HA,63 in the isolated biofilms, we confirmed that both the PA-W23 WT and the pap1 complemented strain had high levels of 6OH-HA in their biofilms, whereas the pap1 biofilm had a 98% reduction in the levels of 6OH-HA (Figures 7A-7C). This indicates that at least part of the increased biofilm phenotype observed for PA-W23 is attributable to the embedding of the PCL breakdown products in the biofilm matrix. There may also be other mechanisms at play, and future work will focus on how the cell senses and responds to the presence of a target plastic substrate and if the integration of the monomer into the biofilm is passive or through direct interactions with the EPS.

Nosocomial pathogens are notorious for their capacity to persist in the hospital-built environment, often surviving on plastic surfaces. This work suggests that pathogens that encode enzymes with the capacity to degrade plastic are better equipped to survive on these hospital plastic surfaces, potentially using the plastic itself as a source for growth or degrading the plastic to form pits, in which the pathogen can shield from traditional surface decontamination procedures. Given the propensity for certain pathogens, such as *P. aeruginosa*, *A. baumannii*, and *Staphylococcus aureus*, to cause persistent outbreaks in hospitals, future infection control strategies may want to consider and determine if outbreak-associated isolates encode plastic-degrading enzymes, augmenting the pathogens' capacity for persistence in the hospital-built environment.

The presence of plastic-degrading bacteria in healthcare is not unexpected. Vast amounts of plastic are present in hospitals. and in the environment, the abundance of plastic-degrading genes is directly linked to the prevalence of plastic pollution. This suggests that exposure to plastic in the hospital setting is driving the adaptation and spread of these enzymes.<sup>2,65</sup> Indeed, we identified several species of clinically relevant bacteria that encode enzymes with the potential to degrade plastic (Table S3). Like antibiotic resistance, if encoding plastic-degrading enzymes confers an advantage to bacterial pathogens, their selection and spread will increase over time. This could be through enzyme evolution, as many plastic-degrading enzymes are similar to lipases and cutinases with other functions that may exhibit substrate promiscuity or through horizontal gene transfer (HGT). 45,66,67 Enzyme evolution and adaptation have been suggested as sources for plastic-degrading enzymes previously, with plastic pollution acting as a recent robust selection pressure. 65 However, HGT likely explains why, for example, we identified a clinical isolate of S. pneumoniae in the genome mining with an almost identical gene to the known functional polyester-degrading enzyme BsEstB. Indeed, we demonstrated that the acquisition of a single pathogen-associated polyesterase was sufficient to confer plastic-degrading activity to P. aeruginosa PA14 and PAO1 (Figure 4B). There is also the threat that some species of environmental bacteria can also be considered opportunistic pathogens, such as *S. stutzeri* (previously *P. stutzeri*).<sup>44</sup> In these instances, it is possible that the bacteria could evolve the capacity to degrade plastic in the environment and then exploit this enzymatic activity to augment virulence in a clinical setting.

Plastic-associated infections, such as catheter-associated urinary tract infections (CA-UTIs) or ventilator-associated pneumonia, are already well known in healthcare, both of which are commonly caused by P. aeruginosa. 68-70 CA-UTIs are responsible for the majority of nosocomial UTIs and represent a significant proportion of healthcare-associated infections, especially bloodstream infections (BSIs).6,7 A particular case study in Quebec found that 21% of healthcare-associated BSIs derived from UTIs, and 71% of these were catheter associated. 71 Patients with CA-UTIs or other device-related infections can experience lengthened the hospital stays, increased risk of re-admission, and increased risk of bacteremia or mortality.  $^{7,9,10,72}$  Due to the significant impact that device-related infections already pose in healthcare, if the causative bacteria were also able to degrade the device and survive off the breakdown products, this could be a previously unrecognized factor significantly impacting patient outcomes.

The genome mining for polyester-degrading homologs in clinical strains found a large number of candidates. However, we discarded many high-similarity hits in pathogenic species that did not provide a detailed isolation source, meaning they may also represent pathogen-associated plastic-degrading enzymes. Future studies will focus on the functional characterization of the lower percentage hits and assessing homologs to all known plastic-degrading enzymes, although most of those currently known are for polyesters, primarily PET.73 Indeed, despite Pap1 being the only enzyme encoded within the PA-W23 genome with any similarity to a known plastic-degrading enzyme, a very faint zone of degradation was still observed in a Δpap1 mutant, suggesting that some other secondary novel enzyme may also be able to act on PCL, although very weakly. However, secretion assays confirmed that the supernatant of the Δpap1 mutant did not have any PCL-degrading activity, conclusively linking the degradation of this polyester to the action of Pap1. We also confirm that Pap1 is secreted in a T2SSdependent manner using a predicted non-canonical SP (Figure 4D). Pap1 is classified as a type IIa PETase-like enzyme except for a change in the sub-site I conserved tryptophan to tyrosine (Y172). We hypothesized that the Y172W variant would have increased activity, given this would revert the Pap1 sub-site I to the classical residue combination for type IIa PETase-like enzymes; however, when tested, it had less activity (Figure 2F), indicating that the PA-W23 WT variant may have evolved to have maximal PCL-degrading activity or potentially be more stable. It is also worth noting that PAO1 produced a residual zone around the colony after 4 days, suggesting some residual PCLdegrading activity (Figure 4B). This could be a promiscuous lipase capable of acting weakly on PCL or a previously uncharacterized PCL-degrading enzyme. Indeed, novel enzymes are constantly being discovered and functionally characterized, which will enlarge the databases for future mining approaches. Even some of the known enzymes are evolutionarily distant





from each other, representing different clades on our phylogenetic tree. Together, this would place human pathogens and clinical isolates as a previously unrecognized reservoir of potential novel plastic-degrading enzymes that could be exploited to create enzyme-based solutions to tackle the plastic waste crisis. Indeed, by screening a clinical isolate collection, we identified an additional strain of *P. aeruginosa* that was capable of degrading plastic and had a similar biofilm response in the presence of PCL.

While the biodegradability of PCL is one of its main advantages for use in healthcare, this could also be its downfall. As it can be degraded by the causative agent of an infection, the potential for increased infection risk and even accelerated degradation of implants or sutures should be considered in device design and treatment planning. Antimicrobial components could be added to PCL medical devices to reduce the risk of infection and biodegradation. Some work on this has already been started, such as composites with silver or copper oxide nanoparticles or electrospinning PCL with halloysite nanotubes impregnated with erythromycin.<sup>74-76</sup> Therefore, implementing this into proposed PCL implanted medical devices should be a priority when considering medical approval and manufacture. While here we only focused on PCL degradation due to its widespread and expanding clinical use, there should also be a consideration for medical devices and implants made from other plastic materials, as many types of plastics have been shown to be degraded by microbes, so these strains could also be present in clinical settings.<sup>35</sup>

#### Limitations of the study

In this work, we focused on demonstrating that Pap1 can degrade the biodegradable plastic PCL. However, it is recognized that some polyesterases can also act on more recalcitrant plastics, such as PET. Indeed, Pap1 has a high level of structural homology to known PET-degrading enzymes such as PET5, suggesting that Pap1 may also be able to degrade PET. Future work will look to explore the spectrum of Pap1 substrate specificity and its regulation. We also did not explore predicted plastic-degrading polyesterases in pathogens other than *P. aeruginosa*. However, this will be the focus of future investigation. There is also a strong likelihood that Pap1 has other functional roles within the cell beyond the degradation of plastic, and we will investigate this in follow-up studies.

We show robust evidence that the capacity for a pathogen to degrade plastic can compromise plastic structural integrity, facilitate pathogen growth and biofilm formation, and increase virulence. Then, it may be necessary to routinely screen pathogens for this ability, particularly in situations where a patient has an infection associated with an implanted plastic device.

#### **RESOURCE AVAILABILITY**

#### **Lead contact**

Further information and requests for resources and reagents should be directed to and will be fulfilled by the lead contact, Prof. Ronan R. McCarthy (ronan.mccarthy@brunel.ac.uk).

#### **Materials availability**

The materials that support the findings of this study are available from the corresponding author upon reasonable request. Please contact the lead contact for additional information.

#### Data and code availability

- RNA-seq data have been deposited at the National Centre for Biotechnology Information Gene Expression Omnibus public database and are publicly available as of the date of publication. Accession numbers are listed in the key resources table.
- This paper does not report original code.
- Any additional information required to reanalyze the data reported in this
  work paper is available from the lead contact upon request.

#### **ACKNOWLEDGMENTS**

We thank Prof. Stephan Heeb for kindly providing the clinical isolate P. aeruginosa PA-W23 and the British Society for Antimicrobial Chemotherapy for providing the BSAC Bacteraemia Resistance Surveillance Programme P. aeruginosa collection. We would like to thank Prof. Alain Filloux for the gift of the different secretion mutants and Dr. Luke Allsopp for retrieving them. R.R.M. and S.A.H. are supported by a National Environmental Research Council Exploring the Frontiers Grant (NE/X010902/1). R.R.M. and R.d.D. are supported by a Biotechnology and Biological Sciences Research Council New Investigator Award (BB/V007823/1) and a Medical Research Council Grant (MR/Y001354/1). R.R.M. is also supported by the Academy of Medical Sciences/the Wellcome Trust/the Government Department of Business, Energy and Industrial Strategy/the British Heart Foundation/Diabetes UK Springboard Award (SBF006\1040). R.R.M. has also received support from the Bio-based Industries Joint Undertaking (JU) under the European Union's Horizon 2020 research and innovation programme under grant agreement no. 887648. The JU receives support from the European Union's Horizon 2020 research and innovation programme and the Bio-based Industries Consortium. R.R.M. and E.M. are also supported by the National Centre for the Replacement, Refinement and Reduction of Animals in Research (NC3Rs) (NC/V001582/1). R.R.M. is also supported by the Biotechnology and Biological Sciences Research Council grant BB/Y008332/1. We thank the Brunel University Experimental Techniques Centre for SEM support. The funders played no role in the study design, data collection, analysis and interpretation of data, or the writing of this manuscript.

#### **AUTHOR CONTRIBUTIONS**

S.A.H., R.d.D., T.H.M., A.M., and R.R.M. designed the study, performed the experiments and analysis, and wrote and revised the manuscript. E.M. performed *Galleria mellonella* experiments and analysis.

#### **DECLARATION OF INTERESTS**

Brunel University London has a priority patent and PCT filings covering the manipulation of biofilm levels to enhance plastic degradation.

#### **STAR**\*METHODS

Detailed methods are provided in the online version of this paper and include the following:

- KEY RESOURCES TABLE
- EXPERIMENTAL MODEL AND STUDY PARTICIPANT DETAILS
  - Microbe strains
- METHOD DETAILS
  - o Genomic mining
  - o Protein bioinformatic analysis
  - o Generation of constructs and plasmid construction
  - o Strain construction
  - o PCL clear zone assay
  - o PCL weight loss and growth curves
  - o Secreted protein fraction precipitation and SDS-PAGE analysis
  - Scanning electron microscopy
  - $\circ\,$  RNA sequencing and differential gene expression analysis
  - Biofilm assay
  - $\,\circ\,$  Animal acquisition and preparation

#### **Article**



- o PCL implant preparation
- o In vivo implant infection assay
- Liquid chromatography-mass spectrometry (LC-MS/MS) analysis of biofilm
- QUANTIFICATION AND STATISTICAL ANALYSIS

#### SUPPLEMENTAL INFORMATION

Supplemental information can be found online at https://doi.org/10.1016/j.celrep.2025.115650.

Received: November 21, 2023 Revised: February 4, 2025 Accepted: April 11, 2025 Published: May 7, 2025

#### **REFERENCES**

- Joseph, B., James, J., Kalarikkal, N., and Thomas, S. (2021). Recycling of medical plastics. Advanced Industrial and Engineering Polymer Research 4, 199–208.
- Czuba, L. (2014). Application of Plastics in Medical Devices and Equipment. In Handbook of Polymer Applications in Medicine and Medical Devices, K. Modjarrad and S. Ebnesajjad, eds. (Elsevier), pp. 9–19.
- Carl, F.H., Richard, M.E., Mark, A.K., and Ross, B. (2014). Endotracheal Tubes: Old and New. Respir. Care 59, 933.
- Rajendran, S., and Anand, S.C. (2020). 11 Woven textiles for medical applications. In Woven Textiles, Second Edition, K.L. Gandhi, ed. (Woodhead Publishing), pp. 441–470.
- Sastri, V.R. (2014). 1 Introduction. In Plastics in Medical Devices, Second Edition, V.R. Sastri, ed. (Oxford: William Andrew Publishing), pp. 1–8.
- Magill, S.S., Edwards, J.R., Bamberg, W., Beldavs, Z.G., Dumyati, G., Kainer, M.A., Lynfield, R., Maloney, M., McAllister-Hollod, L., Nadle, J., et al. (2014). Multistate point-prevalence survey of health care-associated infections. N. Engl. J. Med. 370, 1198–1208.
- Nicolle, L.E. (2014). Catheter associated urinary tract infections. Antimicrob. Resist. Infect. Control 3, 23.
- Pande, T., and Naidu, C.S. (2020). Mesh infection in cases of polypropylene mesh hernioplasty. Hernia 24, 849–856.
- 9. von Eiff, C., Jansen, B., Kohnen, W., and Becker, K. (2005). Infections Associated with Medical Devices. Drugs 65, 179–214.
- VanEpps, J.S., and Younger, J.G. (2016). Implantable Device-Related Infection. Shock 46, 597–608.
- Arciola, C.R., Alvi, F.I., An, Y.H., Campoccia, D., and Montanaro, L. (2005).
   Implant infection and infection resistant materials: a mini review. Int. J. Artif. Organs 28, 1119–1125.
- Bezwada, R.S., Jamiolkowski, D.D., Lee, I.Y., Agarwal, V., Persivale, J., Trenka-Benthin, S., Erneta, M., Suryadevara, J., Yang, A., and Liu, S. (1995). Monocryl suture, a new ultra-pliable absorbable monofilament suture. Biomaterials 16, 1141–1148.
- Niessen, F.B., Spauwen, P.H., and Kon, M. (1997). The role of suture material in hypertrophic scar formation: Monocryl vs. Vicryl-rapide. Ann. Plast. Surg. 39, 254–260.
- Middleton, J.C., and Tipton, A.J. (2000). Synthetic biodegradable polymers as orthopedic devices. Biomaterials 21, 2335–2346.
- 15. Gartti-Jardim, E.C., de Souza, A.P., Carvalho, A.C.G.d.S., Pereira, C.C.S., Okamoto, R., and Magro Filho, O. (2013). Comparative study of the healing process when using Vicryl®, Vicryl Rapid®, Vicryl Plus®, and Monocryl® sutures in the rat dermal tissue. Oral Maxillofac. Surg. 17, 293–298.
- Lotfi, M., Ghasemi, N., Rahimi, S., Vosoughhosseini, S., Saghiri, M.A., and Shahidi, A. (2013). Resilon: a comprehensive literature review. J. Dent. Res. Dent. Clin. Dent. Prospects 7, 119–130.

- Shanahan, D.J., and Duncan, H.F. (2011). Root canal filling using Resilon: a review. Br. Dent. J. 211, 81–88.
- Christen, M.O., and Polycaprolactone, V.F. (2020). How a Well-Known and Futuristic Polymer Has Become an Innovative Collagen-Stimulator in Esthetics. Clin Cosmet Investig Dermatol 13, 31–48.
- 19. de Melo, F., Carrijo, A., Hong, K., Trumbic, B., Vercesi, F., Waldorf, H.A., and Zenker, S. (2020). Minimally Invasive Aesthetic Treatment of the Face and Neck Using Combinations of a PCL-Based Collagen Stimulator, PLLA/PLGA Suspension Sutures, and Cross-Linked Hyaluronic Acid. Clin. Cosmet. Investig. Dermatol. 13, 333–344.
- de Melo, F., Nicolau, P., Piovano, L., Lin, S.L., Baptista-Fernandes, T., King, M.I., Camporese, A., Hong, K., Khattar, M.M., and Christen, M.O. (2017). Recommendations for volume augmentation and rejuvenation of the face and hands with the new generation polycaprolactone-based collagen stimulator (Ellansé(®)). Clin. Cosmet. Investig. Dermatol. 10, 431–440.
- Murab, S., Herold, S., Hawk, T., Snyder, A., Espinal, E., and Whitlock, P. (2023). Advances in additive manufacturing of polycaprolactone based scaffolds for bone regeneration. J. Mater. Chem. B 11, 7250–7279.
- Malikmammadov, E., Tanir, T.E., Kiziltay, A., Hasirci, V., and Hasirci, N. (2018). PCL and PCL-based materials in biomedical applications. J. Biomater. Sci. Polym. Ed. 29, 863–893.
- Woodruff, M.A., and Hutmacher, D.W. (2010). The return of a forgotten polymer—Polycaprolactone in the 21st century. Prog. Polym. Sci. 35, 1217–1256.
- Raina, N., Pahwa, R., Khosla, J.K., Gupta, P.N., and Gupta, M. (2022). Polycaprolactone-based materials in wound healing applications. Polym. Bull. 79, 7041–7063.
- Mosallanezhad, P., Nazockdast, H., Ahmadi, Z., and Rostami, A. (2022). Fabrication and characterization of polycaprolactone/chitosan nanofibers containing antibacterial agents of curcumin and ZnO nanoparticles for use as wound dressing. Front. Bioeng. Biotechnol. 10, 1027351.
- Ng, K.W., Achuth, H.N., Moochhala, S., Lim, T.C., and Hutmacher, D.W. (2007). In vivo evaluation of an ultra-thin polycaprolactone film as a wound dressing. J. Biomater. Sci. Polym. Ed. 18, 925–938.
- Holländer, J., Genina, N., Jukarainen, H., Khajeheian, M., Rosling, A., Mäkilä, E., and Sandler, N. (2016). Three-Dimensional Printed PCL-Based Implantable Prototypes of Medical Devices for Controlled Drug Delivery. J. Pharm. Sci. 105, 2665–2676.
- Boia, R., Dias, P.A.N., Martins, J.M., Galindo-Romero, C., Aires, I.D., Vidal-Sanz, M., Agudo-Barriuso, M., de Sousa, H.C., Ambrósio, A.F., Braga, M.E.M., and Santiago, A.R. (2019). Porous poly(ε-caprolactone) implants: A novel strategy for efficient intraocular drug delivery. J. Control. Release 316. 331–348.
- 29. Bernards, D.A., Bhisitkul, R.B., Wynn, P., Steedman, M.R., Lee, O.T., Wong, F., Thoongsuwan, S., and Desai, T.A. (2013). Ocular biocompatibility and structural integrity of micro- and nanostructured poly(caprolactone) films. J. Ocul. Pharmacol. Ther. 29, 249–257.
- Kim, J., Kudisch, M., Mudumba, S., Asada, H., Aya-Shibuya, E., Bhisitkul, R.B., and Desai, T.A. (2016). Biocompatibility and Pharmacokinetic Analysis of an Intracameral Polycaprolactone Drug Delivery Implant for Glaucoma. Investig. Ophthalmol. Vis. Sci. 57, 4341–4346.
- Dwivedi, R., Kumar, S., Pandey, R., Mahajan, A., Nandana, D., Katti, D.S., and Mehrotra, D. (2020). Polycaprolactone as biomaterial for bone scaffolds: Review of literature. J. Oral Biol. Craniofac. Res. 10, 381–388.
- Ming, H.H.J., W.V.D., Chou, N., and Tsai, T. (2020). Cranial reconstruction using a polycaprolactone implant after burr hole trephination. Journal of 3D Printing in Medicine 4, 9–16.
- Naik, C., Srinath, N., Ranganath, M.K., Umashankar, D.N., and Gupta, H. (2020). Evaluation of polycaprolactone scaffold for guided bone regeneration in maxillary and mandibular defects: A clinical study. Natl. J. Maxillofac. Surg. 11, 207–212.





- 34. Koo, H.T., Oh, J., and Heo, C.Y. (2022). Cranioplasty Using Three-Dimensional-Printed Polycaprolactone Implant and Free Latissimus Dorsi Musculocutaneous Flap in a Patient with Repeated Wound Problem following Titanium Cranioplasty. Arch. Plast. Surg. 49, 740–744.
- 35. Ru, J., Huo, Y., and Yang, Y. (2020). Microbial Degradation and Valorization of Plastic Wastes. Front. Microbiol. 11, 442.
- Groh, K.J., Backhaus, T., Carney-Almroth, B., Geueke, B., Inostroza, P.A., Lennquist, A., Leslie, H.A., Maffini, M., Slunge, D., Trasande, L., et al. (2019). Overview of known plastic packaging-associated chemicals and their hazards. Sci. Total Environ. 651, 3253–3268.
- Freschi, L., Jeukens, J., Kukavica-Ibrulj, I., Boyle, B., Dupont, M.J., Laroche, J., Larose, S., Maaroufi, H., Fothergill, J.L., Moore, M., et al. (2015). Clinical utilization of genomics data produced by the international Pseudomonas aeruginosa consortium. Front. Microbiol. 6, 1036.
- 38. Danso, D., Schmeisser, C., Chow, J., Zimmermann, W., Wei, R., Leggewie, C., Li, X., Hazen, T., and Streit, W.R. (2018). New insights into the function and global distribution of polyethylene terephthalate (PET)-degrading bacteria and enzymes in marine and terrestrial metagenomes. Appl. Environ. Microbiol. 84, e027733-17.
- Joo, S., Cho, I.J., Seo, H., Son, H.F., Sagong, H.-Y., Shin, T.J., Choi, S.Y., Lee, S.Y., and Kim, K.-J. (2018). Structural insight into molecular mechanism of poly(ethylene terephthalate) degradation. Nat. Commun. 9, 382.
- Perez-Garcia, P., Chow, J., Costanzi, E., Gurschke, M., Dittrich, J., Dierkes, R.F., Molitor, R., Applegate, V., Feuerriegel, G., Tete, P., et al. (2023). An archaeal lid-containing feruloyl esterase degrades polyethylene terephthalate. Commun. Chem. 6, 193.
- 41. Zhang, H., Dierkes, R.F., Perez-Garcia, P., Costanzi, E., Dittrich, J., Cea, P. A., Gurschke, M., Applegate, V., Partus, K., Schmeisser, C., et al. (2023). The metagenome-derived esterase PET40 is highly promiscuous and hydrolyses polyethylene terephthalate (PET). FEBS J. 291, 70–91.
- Howard, S.A., and McCarthy, R.R. (2023). Modulating biofilm can potentiate activity of novel plastic-degrading enzymes. NPJ Biofilms Microbiomes 9, 72.
- Nakamura, A., Kobayashi, N., Koga, N., and lino, R. (2021). Positive Charge Introduction on the Surface of Thermostabilized PET Hydrolase Facilitates PET Binding and Degradation. ACS Catal. 11, 8550–8564.
- 44. Alwazzeh, M.J., Alkuwaiti, F.A., Alqasim, M., Alwarthan, S., and El-ghoneimy, Y. (2020). Infective Endocarditis Caused by Pseudomonas stutzeri: A Case Report and Literature Review. Infect. Dis. Rep. 12, 105–109.
- Wilkes, R.A., and Aristilde, L. (2017). Degradation and metabolism of synthetic plastics and associated products by Pseudomonas sp.: capabilities and challenges. J. Appl. Microbiol. 123, 582–593.
- Bleves, S., Viarre, V., Salacha, R., Michel, G.P.F., Filloux, A., and Voulhoux, R. (2010). Protein secretion systems in Pseudomonas aeruginosa: A wealth of pathogenic weapons. Int. J. Med. Microbiol. 300, 534–543. https://doi.org/10.1016/j.ijmm.2010.08.005.
- Chen, L., and Wen, Y.M. (2011). The role of bacterial biofilm in persistent infections and control strategies. Int. J. Oral Sci. 3, 66–73.
- Leid, J.G. (2009). Bacterial biofilms resist key host defenses. Microbe 4 66–70
- Liao, C., Huang, X., Wang, Q., Yao, D., and Lu, W. (2022). Virulence Factors of Pseudomonas Aeruginosa and Antivirulence Strategies to Combat Its Drug Resistance. Front. Cell. Infect. Microbiol. 12, 926758.
- Campos-Silva, R., Brust, F.R., Trentin, D.S., and Macedo, A.J. (2019).
   Alternative method in Galleria mellonella larvae to study biofilm infection and treatment. Microb. Pathog. 137, 103756.
- Thi, M.T.T., Wibowo, D., and Rehm, B.H.A. (2020). Pseudomonas aeruginosa Biofilms. Int. J. Mol. Sci. 21, 8671.
- McCarthy, R.R., Mazon-Moya, M.J., Moscoso, J.A., Hao, Y., Lam, J.S., Bordi, C., Mostowy, S., and Filloux, A. (2017). Cyclic-di-GMP regulates lipopolysaccharide modification and contributes to Pseudomonas aeruginosa immune evasion. Nat. Microbiol. 2, 17027.

- Mah, T.-F., Pitts, B., Pellock, B., Walker, G.C., Stewart, P.S., and O'Toole, G.A. (2003). A genetic basis for Pseudomonas aeruginosa biofilm antibiotic resistance. Nature 426, 306–310.
- 54. Ciofu, O., and Tolker-Nielsen, T. (2019). Tolerance and Resistance of Pseudomonas aeruginosa Biofilms to Antimicrobial Agents-How P. aeruginosa Can Escape Antibiotics. Front. Microbiol. 10, 913.
- 55. Alhede, M., Bjarnsholt, T., Givskov, M., and Alhede, M. (2014). Chapter One - Pseudomonas aeruginosa Biofilms: Mechanisms of Immune Evasion. In Advances in Applied Microbiology, 86, S. Sariaslani and G. M. Gadd, eds. (Academic Press), pp. 1–40.
- Byrd, M.S., Pang, B., Hong, W., Waligora, E.A., Juneau, R.A., Armbruster, C.E., Weimer, K.E.D., Murrah, K., Mann, E.E., Lu, H., et al. (2011). Direct Evaluation of Pseudomonas aeruginosa Biofilm Mediators in a Chronic Infection Model. Infect. Immun. 79, 3087–3095.
- Wagner, V.E., and Iglewski, B.H. (2008). aeruginosa Biofilms in CF Infection. Clin. Rev. Allergy Immunol. 35, 124–134.
- Basili, M., Quero, G.M., Giovannelli, D., Manini, E., Vignaroli, C., Avio, C.G., De Marco, R., and Luna, G.M. (2020). Major Role of Surrounding Environment in Shaping Biofilm Community Composition on Marine Plastic Debris. Front. Mar. Sci. 7, 262.
- Lobelle, D., and Cunliffe, M. (2011). Early microbial biofilm formation on marine plastic debris. Mar. Pollut. Bull. 62, 197–200.
- Morohoshi, T., Oi, T., Aiso, H., Suzuki, T., Okura, T., and Sato, S. (2018).
   Biofilm Formation and Degradation of Commercially Available Biodegradable Plastic Films by Bacterial Consortiums in Freshwater Environments.
   Microbes Environ. 33, 332–335.
- Gilan, I., Hadar, Y., and Sivan, A. (2004). Colonization, biofilm formation and biodegradation of polyethylene by a strain of Rhodococcus ruber. Appl. Microbiol. Biotechnol. 65, 97–104.
- Liu, S.Y., Leung, M.M.L., Fang, J.K.H., and Chua, S.L. (2021). Engineering a microbial 'trap and release' mechanism for microplastics removal. Chem. Eng. J. 404, 127079.
- Heimowska, A., Morawska, M., and Bocho-Janiszewska, A. (2017). Biodegradation of poly(e-caprolactone) in natural water environments. Pol. J. Chem. Technol. 19, 120–126. https://doi.org/10.1515/pjct-2017-0017.
- 64. Vickery, K., Deva, A., Jacombs, A., Allan, J., Valente, P., and Gosbell, I.B. (2012). Presence of biofilm containing viable multiresistant organisms despite terminal cleaning on clinical surfaces in an intensive care unit. J. Hosp. Infect. 80, 52–55.
- Zrimec, J., Kokina, M., Jonasson, S., Zorrilla, F., Zelezniak, A., Kelly, L., and Newman, D.K. (2021). Plastic-Degrading Potential across the Global Microbiome Correlates with Recent Pollution Trends. mBio 12, e02155-21.
- Newton, M.S., Arcus, V.L., Gerth, M.L., and Patrick, W.M. (2018). Enzyme evolution: innovation is easy, optimization is complicated. Curr. Opin. Struct. Biol. 48, 110–116.
- Boto, L. (2010). Horizontal gene transfer in evolution: facts and challenges. Proc. Biol. Sci. 277, 819–827.
- Newman, J.N., Floyd, R.V., and Fothergill, J.L. (2022). Invasion and diversity in Pseudomonas aeruginosa urinary tract infections. J. Med. Microbiol. 71, 001458.
- Newman, J.W., Floyd, R.V., and Fothergill, J.L. (2017). The contribution of Pseudomonas aeruginosa virulence factors and host factors in the establishment of urinary tract infections. FEMS Microbiol. Lett. 364, fnx124.
- Ramírez-Estrada, S., Borgatta, B., and Rello, J. (2016). Pseudomonas aeruginosa ventilator-associated pneumonia management. Infect. Drug Resist. 9, 7–18.
- Fortin, E., Rocher, I., Frenette, C., Tremblay, C., and Quach, C. (2012).
   Healthcare-Associated Bloodstream Infections Secondary to a Urinary Focus The Québec Provincial Surveillance Results. Infect. Control Hosp. Epidemiol. 33, 456–462.

#### **Article**



- Judy, J., Baumer, D., and Khoo, C. (2021). Descriptive Analysis of Healthcare Resource Utilization and Costs Associated with Treatment of Urinary Tract Infections in United States Hospitals. Am. J. Infect. Control 49, S2.
- Buchholz, P.C.F., Feuerriegel, G., Zhang, H., Perez-Garcia, P., Nover, L.L., Chow, J., Streit, W.R., and Pleiss, J. (2022). Plastics degradation by hydrolytic enzymes: The plastics-active enzymes database-PAZy. Proteins 90, 1443–1456.
- Tran, P.A., Hocking, D.M., and O'Connor, A.J. (2015). In situ formation of antimicrobial silver nanoparticles and the impregnation of hydrophobic polycaprolactone matrix for antimicrobial medical device applications. Mater. Sci. Eng. C 47, 63–69.
- Balcucho, J., Narváez, D.M., and Castro-Mayorga, J.L. (2020). Antimicrobial and Biocompatible Polycaprolactone and Copper Oxide Nanoparticle Wound Dressings against Methicillin-Resistant Staphylococcus aureus. Nanomaterials 10. 1692.
- Khunová, V., Kováčová, M., Olejniková, P., Ondreáš, F., Špitalský, Z., Ghosal, K., and Berkeš, D. (2022). Antibacterial Electrospun Polycaprolactone Nanofibers Reinforced by Halloysite Nanotubes for Tissue Engineering. Polymers 14, 746.
- Durand, E., Bernadac, A., Ball, G., Lazdunski, A., Sturgis, J.N., and Filloux, A. (2003). Type II protein secretion in Pseudomonas aeruginosa: the pseudopilus is a multifibrillar and adhesive structure. J Bacteriol 185, 2749–2758.
- Soscia, C., Hachani, A., Bernadac, A., Filloux, A., and Bleves, S. (2007).
   Cross talk between type III secretion and flagellar assembly systems in Pseudomonas aeruginosa. J Bacteriol 189, 3124–3132.
- Garnett, J.A., Muhl, D., Douse, C.H., Hui, K., Busch, A., Omisore, A., Yang, Y., Simpson, P., Marchant, J., Waksman, G., et al. (2015). Structurefunction analysis reveals that the Pseudomonas aeruginosa Tps4 twopartner secretion system is involved in CupB5 translocation. Protein Sci. 24, 670–687.
- de Dios, R., Gadar, K., and McCarthy, R.R. (2022). A high-efficiency scarfree genome-editing toolkit for Acinetobacter baumannii. J. Antimicrob. Chemother. 77, 3390–3398.
- WHO (2017). Global priority list of antibiotic-resistant bacteria to guide research. In Discovery, and Development of New Antibiotics.
- Haque, M., Sartelli, M., McKimm, J., and Abu Bakar, M. (2018). Health care-associated infections - an overview. Infect. Drug Resist. 11, 2321–2333.
- Carr, C.M., Clarke, D.J., and Dobson, A.D.W. (2020). Microbial Polyethylene Terephthalate Hydrolases: Current and Future Perspectives. Front. Microbiol. 11, 571265.

- Paysan-Lafosse, T., Blum, M., Chuguransky, S., Grego, T., Pinto, B.L., Salazar, G.A., Bileschi, M.L., Bork, P., Bridge, A., Colwell, L., et al. (2023). InterPro in 2022. Nucleic Acids Res. 51, D418–D427.
- 85. Teufel, F., Almagro Armenteros, J.J., Johansen, A.R., Gíslason, M.H., Pihl, S.I., Tsirigos, K.D., Winther, O., Brunak, S., von Heijne, G., and Nielsen, H. (2022). SignalP 6.0 predicts all five types of signal peptides using protein language models. Nat. Biotechnol. 40, 1023–1025.
- Bendtsen, J.D., Kiemer, L., Fausbøll, A., and Brunak, S. (2005). Non-classical protein secretion in bacteria. BMC Microbiol. 5, 58.
- 87. Madeira, F., Pearce, M., Tivey, A.R.N., Basutkar, P., Lee, J., Edbali, O., Madhusoodanan, N., Kolesnikov, A., and Lopez, R. (2022). Search and sequence analysis tools services from EMBL-EBI in 2022. Nucleic Acids Res. 50, W276–W279.
- Waterhouse, A.M., Procter, J.B., Martin, D.M.A., Clamp, M., and Barton, G.J. (2009). Jalview Version 2—a multiple sequence alignment editor and analysis workbench. Bioinformatics 25, 1189–1191.
- Kelley, L.A., Mezulis, S., Yates, C.M., Wass, M.N., and Sternberg, M.J.E. (2015). The Phyre2 web portal for protein modeling, prediction and analvsis. Nat. Protoc. 10. 845–858.
- Meisner, J., and Goldberg, J.B. (2016). The Escherichia coli rhaSR-Prha-BAD Inducible Promoter System Allows Tightly Controlled Gene Expression over a Wide Range in Pseudomonas aeruginosa. Appl. Environ. Microbiol. 82, 6715–6727.
- Figurski, D.H., and Helinski, D.R. (1979). Replication of an origin-containing derivative of plasmid RK2 dependent on a plasmid function provided in trans. Proc. Natl. Acad. Sci. USA 76, 1648–1652.
- Choi, K.-H., Gaynor, J.B., White, K.G., Lopez, C., Bosio, C.M., Karkhoff-Schweizer, R.R., and Schweizer, H.P. (2005). A Tn7-based broad-range bacterial cloning and expression system. Nat. Methods 2, 443–448.
- 93. Almeida, E.L., Carrillo, R.A.F., Jackson, S.A., and Dobson, A.D.W. (2019). In silico Screening and Heterologous Expression of a Polyethylene Terephthalate Hydrolase (PETase)-Like Enzyme (SM14est) With Polycaprolactone (PCL)-Degrading Activity, From the Marine Sponge-Derived Strain Streptomyces sp. SM14. Front. Microbiol. 10, 2187.
- Howard, S.A., Carr, C.M., Sbahtu, H.I., Onwukwe, U., López, M.J., Dobson, A.D.W., and McCarthy, R.R. (2023). Enrichment of native plastic-associated biofilm communities to enhance polyester degrading activity. Environ. Microbiol. 25, 2698–2718.
- Flaugnatti, N., and Journet, L. (2017). Identification of Effectors: Precipitation of Supernatant Material. Methods Mol. Biol. 1615, 459–464.





#### **STAR**\*METHODS

#### **KEY RESOURCES TABLE**

REAGENT or RESOURCE	SOURCE	IDENTIFIER
Bacterial strains		
E. coli strain BL21 Star™ (DE3) pLysS	Invitrogen	Cat number: C602003
P. aeruginosa strain PA-W23	Dr Stephan Heeb's collection, University of Nottingham	GCF_003833705.1
P. aeruginosa strain PA14	Laboratory collection	GCF_000014625.1
P. aeruginosa strain PAO1	Prof A. Filloux's collection, Imperial College London	GCF_000001405.40
P. aeruginosa strain PAO1 ΔxcpA	Durand et al. <sup>77</sup>	N/A
P. aeruginosa strain PAO1 ΔpscN	Soscia et al. <sup>78</sup>	N/A
P. aeruginosa strain PAO1 ΔpilAΔfliCΔtpsB4	Garnett et al. <sup>79</sup>	N/A
P. aeruginosa strain PA-W23 Δpap1	This work	N/A
P. aeruginosa strain PA14/miniTn7-Gm- lacl <sup>q</sup> -Ptac-Pap1_noSP	This work	N/A
<i>P. aeruginosa</i> strain PA14/miniTn7-Gm- lacl <sup>q</sup> -Ptac	This work	N/A
P. aeruginosa strain PA-W23/miniTn7-Gm- lacl <sup>q</sup> -Ptac-Pap1_noSP	This work	N/A
P. aeruginosa strain PA-W23/miniTn7-Gm- lacI <sup>q</sup> -Ptac	This work	N/A
P. aeruginosa strain PA-W23 Δpap1/ miniTn7-Gm-lacl <sup>q</sup> -Ptac-Pap1_noSP	This work	N/A
<i>P. aeruginosa</i> strain PA-W23 Δ <i>pap1/</i> miniTn7-Gm-lacl <sup>q</sup> -Ptac	This work	N/A
Chemicals, peptides, and recombinant proteins		
LB broth Miller (Luria-Bertani)	Difco, Fisher	Cat number: BD 244620
Agar-agar	Sigma-Aldrich	Cat number: 05039
Polycaprolactone Mn 80,000	Sigma-Aldrich	Cat number: 440744
M9 minimal medium salts	MP Biomedicals	Cat number: 3037032
Pseudomonas isolation agar	Merck	Cat Number: 17208-500G
PageRuler Plus Prestained Protein Lader	Fisher Scientific	Cat Number: 26619
EZBlue Coomassie Brilliant Blue	Merck	Cet Number: G1041-500ML
Deposited data		
P. aeruginosa PA-W23 RNA-Seq data	Gene Expression Omnibus	GSE275972
Oligonucleotides		
pap1 fw Pstl	Integrated DNA Technologies	N/A
pap1 rv HindIII	Integrated DNA Technologies	N/A
pap1 up fw	Integrated DNA Technologies	N/A
pap1 up rv	Integrated DNA Technologies	N/A
pap1 down fw	Integrated DNA Technologies	N/A
pap1 down rv	Integrated DNA Technologies	N/A
Recombinant DNA		
pET-20b(+)-pap1_SP	GenScript	Gene accession RPM52859.1
pET-20b(+)- <i>pap1</i> _noSP	GenScript, His Tag added	N/A
pET-20b(+)- <i>pap1</i> _SP_Y172W	GenScript	N/A
pUC18T-miniTn7T-Gm-lacl <sup>q</sup> -Ptac	AddGene	#110558
(pJM101) pJM101 <i>-pap1</i> _noSP	This work, His Tag added.	N/A

(Continued on next page)

#### **Article**



Continued		
REAGENT or RESOURCE	SOURCE	IDENTIFIER
pEMGT	de Dios et al. (2022) <sup>80</sup>	N/A
pEMGT-pap1	This work	N/A
pRK2013	Laboratory collection	N/A
pTNS2	Laboratory collection	N/A
Software and algorithms		
Protein BLAST	NCBI	https://blast.ncbi.nlm.nih.gov/Blast.cgi? PAGE=Proteins
InterPro	EMBL-EBI	https://www.ebi.ac.uk/interpro/
SignalP (version 6)	DTU Health Tech	https://services.healthtech.dtu.dk/ services/SignalP-6.0/
SecretomeP (version 2)	DTU Health Tech	https://services.healthtech.dtu.dk/ services/SecretomeP-2.0/
EMBOSS Needle	EMBL-EBI	https://www.ebi.ac.uk/Tools/psa/emboss_needle/
Jalview	The Barton Group, University of Dundee	https://www.jalview.org/download/
Phyre2	Genome 3D	http://www.sbg.bio.ic.ac.uk/~phyre2/html/page.cgi?id=index
PyMOL	Schrödinger, LLC	https://pymol.org sales@schrodinger.com
MEGA (version 11.0.11)	MEGA	https://www.megasoftware.net
iTOL (version 6.8.1)	iTOL	https://itol.embl.de
Graphpad Prism (version 10.0.3)	GraphPad Software	https://www.graphpad.com

#### **EXPERIMENTAL MODEL AND STUDY PARTICIPANT DETAILS**

#### Microbe strains

Bacterial strains (E. coli strain BL21 StarTM (DE3) pLysS, P. aeruginosa strain PA-W23, P. aeruginosa strain PA14, P. aeruginosa strain PAO1, P. aeruginosa strain PAO1 ΔxcpA, P. aeruginosa strain PAO1 ΔpilAΔfliCΔtpsB4, P. aeruginosa strain PA-W23 Δpap1, P. aeruginosa strain PA14/miniTn7-Gm-laclq-Ptac-Pap1\_noSP, P. aeruginosa strain PA14/miniTn7-Gm-laclq-Ptac-Pap1\_noSP, P. aeruginosa strain PA-W23/miniTn7-Gm-laclq-Ptac-Pap1\_noSP, P. aeruginosa strain PA-W23/miniTn7-Gm-laclq-Ptac, P. aeruginosa strain PA-W23 Δpap1/miniTn7-Gm-laclq-Ptac-Pap1\_noSP, P. aeruginosa strain PA-W23 Δpap1/miniTn7-Gm-laclq-Ptac) were grown at 37°C throughout (unless otherwise indicated), liquid cultures were grown with agitation at 180 rpm. Growth of strains was performed in lysogeny broth (LB) (Miller formulation) unless otherwise stated.

#### **METHOD DETAILS**

#### **Genomic mining**

A list of 19 pathogenic bacterial species were generated (Table S1) from the WHO's Priority Pathogen list and common healthcare-associated pathogens<sup>81,82</sup> and 23 known polyester-degrading enzymes (Table S2) were collated. Table S2 he known polyester-degrading enzyme protein sequences were used to search for novel potentially polyester-degrading enzymes using NCBI Protein Blast of the non-redundant protein sequences database, the organism selection was limited to those species listed in Table S1. BLAST hits were then investigated for isolation sources that are linked to pathogenesis or clinical isolates, such as isolation from wounds or human anatomical site.

#### **Protein bioinformatic analysis**

InterPro<sup>84</sup> was used to analyze Pap1 protein sequence for known domains and families. Signal peptides were predicted with SignalP - 6.0 and SecretomeP 2.0.<sup>85,86</sup> EMBOSS Needle pairwise alignment<sup>87</sup> was used to align Pap1 and PET5, Jalview 2.11.2.7<sup>88</sup> was used to color the alignment by conservation. Phyre2<sup>89</sup> was used to predict the Pap1 protein structure and PyMOL was used for visualisation and alignment using command 'cealign'. MEGA (version 11.0.11) was used for phylogenetic tree construction; alignment was performed using the MUSCLE algorithm, distance was measured using pairwise *p*-distance with standard settings, a neighbour-joining tree was constructed using *p*-distance with standard settings. iTOL (version 6.8.1) was used to color code the trees.





#### Generation of constructs and plasmid construction

The different versions of the Pap1 coding gene were generated and cloned into pET20b by GenScript (Oxford, UK). The sequences were codon-optimised for expression in *E. coli*. Pap1 was cloned using EcoRV to use the pET20b *pelB* leader sequence to generate Pap1\_SP since no traditional signal peptide was present. A Pap1 version without *pelB* signal peptide and bearing a 6xHis tag in the N terminus was cloned in pET20b using the Ndel and Xhol restriction sites, yielding the Pap1\_noSP construct. A Pap1 version (including *pelB* signal peptide) with the tyrosine in position 172 changed to tryptophan was cloned into pET20b using the EcoRV and Xhol restriction sites, generating the Pap1\_SP\_Y172W construct. *E. coli* BL21 Star (DE3) pLysS was used for expression with ampicillin 100 μg/mL for pET20b plasmid selection and maintenance.

To express *pap1* in *P. aeruginosa*, the Pap1\_noSP construct was subcloned into pUC18T-miniTn7T-Gm-lacl<sup>q</sup>-Ptac (pJM101), which was used to generate a stable miniTn7 chromosomal insertion in the neutral *att*Tn7 site. The Pap1\_noSP construct was amplified from pET20b-Pap1\_noSP using the oligonucleotides pap1 fw Pstl (TTTTCTGCAGAGACCACACGGTTTCCCTC) and pap1 rv HindIII (TTTTTAAGCTTTGTTAGCAGCCGGATCTCAG). The PCR product was digested with Pstl and HindIII and the resulting fragment was cloned into pJM101 cut with the same enzymes, generating pJM101- Pap1\_noSP.

To delete *pap1* from *P. aeruginosa* PA-W23, the *pap1* upstream and downstream homologous regions (approx. 1 kb each) were amplified using the primer pairs pap1 up fw/pap1 up rv (CCTTGCAGGCATAGGTCTTG/GCAAAGTATGCGCTCCATAG) and pap1 down fw/pap1 down rv (CTATGGAGCGCATACTTTGCGAAAACTGCGACTACTGACC/AAGTCGTCCTTGGTGATCAG), respectively. Both homologous regions were joined by sewing PCR and cloned into pEMGT<sup>80</sup> cut with Small to generate pEMGT-pap1. All in-house generated constructs were validated by Sanger sequencing.

#### **Strain construction**

To construct a P. aeruginosa PA-W23  $\Delta pap1$  mutant, we followed the Scel-mediated genome editing protocol established by de Dios et al. (2022)<sup>80</sup> with modifications. Briefly, pEMGT-pap1 was introduced in PA-W23 via triparental mating using pRK2013<sup>91</sup> as helper plasmid and recombinant transconjugants were selected on Pseudomonas isolation agar supplemented with kanamycin 2000  $\mu$ g/mL incubated at 30°C overnight. An isolated transconjugant was used in a second triparental conjugation to introduce pSW-Apr (carrying the endonuclease Scel coding gene under a 3-methylbenzoate-inducible promoter) and trigger a second recombination that would result in the deletion of pap1. The transconjugants were plated on Pseudomonas isolation agar supplemented with apramycin 200  $\mu$ g/mL (for selection of transconjugants) and 3-methylbenzoate 15 mM (to induce the expression of Scel and trigger the second recombination) and incubated at 30°C overnight. The resulting PA-W23  $\Delta pap1$  mutant was validated by PCR and Sanger sequencing. After this validation, the pSW-Apr plasmid was cured by serial passaging in LB broth in the absence of antibiotics.

To introduce pJM101 (empty vector control) and pJM101-Pap1\_noSP into *P. aeruginosa* PA14, wild type PA-W23 and the PA-W23  $\Delta$ pap1 mutant and generate miniTn7-derivative insertions, we followed the four-parental mating protocol established by Choi et al. (2005), <sup>92</sup> using pRK2013 (conjugation helper) and pTNS2 (transposition helper) as helper plasmids. Transconjugants carrying the miniTn7-derivative insertions were selected on *Pseudomonas* isolation agar supplemented with gentamycin 20  $\mu$ g/mL or 100  $\mu$ g/mL for PA14 or PA-W23, respectively, and incubated at 30°C overnight. The miniTn7 insertions were validated by PCR.

#### PCL clear zone assay

PCL (Sigma-Aldrich, Mn 80,000) was dissolved in acetone with agitation at  $50^{\circ}$ C then mixed with LB agar solution (distilled water, 1.5% w/v agar-agar, 2% w/v LB medium) to a concentration of 1% w/v PCL after acetone evaporatio.  $^{93,94}$  After autoclaving, the agar was cooled slightly (but not solidified to keep PCL in solution), Ampicillin 100  $\mu$ g/mL and 0.5 mM Isopropyl  $\beta$ -D-1-thiogalactopyranoside (IPTG) were added where appropriate for *E. coli* BL21 Star (DE3) pLysS clear zone assays, and poured into plates, resulting in cloudy agar plates. Overnight cultures of bacteria grown in LB were OD corrected to OD<sub>600</sub> 3.0, 20  $\mu$ L of this was spotted onto the 1% PCL LBA plates and grown at 37°C, with measurements of the diameter of the bacterial colony and zone of clearance (transparent agar surrounding colony) taken over four days.  $^{94}$ 

To assay the PCL degradation activity of cell-free P. aeruginosa supernatants, 5 mL of LB broth (supplemented with IPTG 1 mM when necessary) were inoculated with the strain of interest. The cultures were incubated at  $37^{\circ}$ C, 180 rpm for 18 h. After this incubation, 1 mL of culture was centrifuged 3 min, 8,000 g, and the cleared supernatant was flushed through a 0.22  $\mu$ m syringe filter. 30  $\mu$ L of each tested cell-free supernatant were spotted on a plain PCL LB agar plate, left to air-dry and incubated at  $37^{\circ}$ C. The clear degradation zones were photographed after 6 h of incubation.

#### PCL weight loss and growth curves

For PCL weight loss assays in LB, overnight cultures grown in LB broth at  $37^{\circ}$ C were used to inoculate 10 mL fresh LB at  $OD_{600}$  0.1 containing 10 sterilised (using 70% industrial methylated spirit (IMS)) and weighed PCL beads ( $\sim$ 0.19 g). For PCL weight loss assays in M9 minimal media with no carbon source (1x M9 salts, 2mM MgSO<sub>4</sub>, 0.1mM CaCl<sub>2</sub>), overnight cultures grown in LB broth at  $37^{\circ}$ C were centrifuged, supernatant removed and resuspended in PBS three times to remove residual LB media. The final pellet was then resuspended in M9 minimal media and used to inoculate 10 mL fresh M9 minimal media at  $OD_{600}$  0.5 for PA-W23 and 0.1 for PA14, containing 10 sterilised and weighed PCL beads, and grown at  $37^{\circ}$ C with agitation. The PA-W23 M9 minimal media cultures were also used for growth curves, with  $OD_{600}$  readings taken at day 0 (after inoculation), day 5, 10 and 14. At the end of the assay, the PCL beads were collected using a fine mesh sieve ( $63 \,\mu$ m), rinsed with distilled water, washed on a room temperature rocker in 2% sodium

## **Cell Reports**Article



dodecyl sulfate overnight to remove biofilm, rinsed with distilled water and dried before being weighed. Control weight loss flasks with uninoculated media and PCL were used to correct the weight loss measurements to account for instrument error so that the control had 0% weight loss.

To test any potential growth defect of the PA-W23  $\Delta pap1$  mutant with respect to the wild type parental strain, we performed growth curve assays in 20 mL of LB in the presence and absence of PCL (1 PCL bead per mL of media). Overnight cultures of each strain were diluted to  $OD_{600}$  0.1 and the cultures were incubated at 37°C, 180 rpm. The  $OD_{600}$  of the cultures was monitored every hour during 8 h and 24 h after starting the growth.

#### Secreted protein fraction precipitation and SDS-PAGE analysis

To test the secretion of Pap1, and hence its presence in the culture supernatant after cell growth, we aimed to isolate the secreted protein fraction and directly visualise it through SDS-PAGE. For this, we followed a pipeline based on the protocol described in Flaugnatti and Jouret (2017)95 that included growing the P. aeruginosa strains of interest, harvesting cell-free supernatant from those cultures, concentrating the protein content of the cell-free supernatant through protein precipitation and direct visualisation of the secreted protein content by SDS-PAGE and Coomassie stain. The P. aeruginosa strains of interest were grown in 5 mL LB (supplemented or not with IPTG 1 mM) during 18 h (37°C, 180 rpm). Once grown, the supernatant of the cultures was harvested by centrifugation (3 min, 10,000 g; a second centrifugation was performed to further clear the supernatants) and cell-free supernatants were obtained by passing them through a 0.22 µm syringe filter. The protein content of the resulting cell-free supernatants (secreted protein fraction) was precipitated by mixing them with trichloroacetic acid (TCA) at a final concentration of 20% and incubating them on ice at 4°C overnight. The precipitated secreted protein fractions were centrifuged (4°C, 30 min, 21,000 g) and the protein pellets were washed twice with 500 μL of ice-cold acetone, centrifuged (4°C, 15 min, 21,000 q) and air-dried in a laminar flow cabinet. For normalisation of the protein content, the secreted protein pellets were resuspended in 2 μL of protein loading buffer 1X [Tris-HCl 80 mM pH 8.0, glycerol 10% (v/v), SDS 2% (w/v), bromophenol blue 0.05% (w/v), β-mercaptoethanol 5% (v/v)] per original OD<sub>600</sub> unit of the culture used for precipitation (i.e., volume of supernatant used for TCA precipitation multiplied by the original  $OD_{600}$  of the culture). Once fully resuspended, the samples were processed for SDS-PAGE by incubating at 100°C during 5 min and centrifuged 3 min, 15,000 g. 5 µL of each sample were run through an SDS-PAGE 12.5% acrylamide gel and stained with Coomassie blue (EZBlue) according to the manufacturer's instructions. The resulting protein gels were imaged with a G:Box F3 imager (Syngene).

#### Scanning electron microscopy

PCL beads from the PA-W23 7-day LB weight loss assay were analyzed using SEM. PCL beads were gold coated for 135 s and imaged with EHT of 5 kV, magnifications of 40, 100, 500 and 1000 were used.

#### RNA sequencing and differential gene expression analysis

Cells were grown to mid-exponential phase (OD<sub>600</sub> 0.6–0.7) in 20 mL Starvation media (10% LB + 90% M9 Minimal Media) supplemented with 0.5 g of PCL beads in the treated samples in biological triplicate. Cells were spun down and washed in RNAlater to preserve RNA integrity. RNA was isolated using the RNAeasy Kit with on-column DNAase digestion (Qiagen). RNA integrity was determined using a Bioanalyzer. Samples were further processed for RNA sequencing on an Illumina MiSeq with 12 million reads per sample. Sequencing and downstream analyses were performed at Microbial Genome Sequencing Center (Pittsburgh, Pennsylvania, U.S.A). Quality control and adapter trimming was performed with bcl2fastq. Read mapping were performed with HISAT. Differential expression analysis was performed using the edgeR's exact test for differences between two groups of negative-binomial counts with an estimated dispersion value of 0.1. and using the P. aeruginosa PA-W23 genome annotation as reference (GCA\_003833705.1). Genes were defined as differentially expressed if Log2(fold change) > 1 or < -1 and p value <0.05.

#### **Biofilm assay**

A pipeline for this assay is summarised in Figure S4. Overnight cultures grown in LB broth at  $37^{\circ}$ C were  $OD_{600}$  corrected to  $OD_{600}$  0.1 in 1 mL fresh LB, 150  $\mu$ L of this was added to each of six wells of a 96-well flat-bottomed plate, with three of the wells containing a sterile PCL or glass bead. The 96-well plate was incubated with agitation at  $37^{\circ}$ C for 24 h. The cultures and PCL beads were removed, and plate washed 3 times with distilled water, 200  $\mu$ L 0.1% crystal violet was added to each well for 12 min then removed, and the plate was washed 5 times with distilled water. The plates were fully air dried at room temperature then 200  $\mu$ L 99% ethanol added to each well to dissolve the crystal violet for 4 h at room temperature. The plate was then read on a plate reader at 570 nm. For 6OH-HA supplementation assays the above procedure was followed with the exception that 200  $\mu$ L was used and 2.17 mg/mL of 6OH-HA added at the beginning of the assay. For CFU analysis, after 24 h growth with and without a PCL bead in a 96-well plate, serial dilutions were made in PBS from the culture and spotted in triplicate on LBA plates, grown overnight at  $37^{\circ}$ C then counted.

#### **Animal acquisition and preparation**

Galleria mellonella larvae were sourced from UK Waxworms Ltd (Dinnington, Sheffield). The animals were at a stage in their life cycle (6<sup>th</sup> instar) where they do not need to be fed. Prior to use the larvae were kept in plastic containers with wood shavings and were





stored at  $+4^{\circ}$ C to minimise the larval movement during procedure. The larvae were sorted into Petri dishes lined with filter paper (Whatman) ensuring all larvae are above 200 mg in weight, which is consistent with them reaching full adulthood and show no signs of melanization. 10 larvae were allowed per Petri dish.

#### **PCL** implant preparation

The implants were created from melting PCL (Sigma-Aldrich, Mn 80,000) into a sheet using a heat block at 85°C. Pieces weighing between 5 mg and 7 mg were measured and cut out of the sheet of PCL. Each piece was laid between two sheets of aluminum foil and heated to 85°C on a heat block to soften the plastic. Once mouldable, the piece was rolled into a 11 mm rod by hand and left to cool and solidify. The cooled rod implants were then sterilised in 70% IMS for 5 min, the IMS was then aspirated and the implants dried for 1 h in the sterile laminar flow hood. Prior to the procedure, the number of sewing pins equal to the number of larvae used for the experiment was placed in a Petri dish and soaked in 70% IMS at least for 30 min to sterilise.

#### In vivo implant infection assay

*P. aeruginosa* PA14 and *P. aeruginosa* PA-W23 were grown at  $37^{\circ}$ C overnight. The cultures were standardised to  $0D_{600} = 1$  and washed 3 times in PBS. The cultures were then serially diluted to  $10^{-6}$ . The larvae were taken out of the  $4^{\circ}$ C incubator and sprayed with 70% IMS to sterilise their surface. A puncture was made in the  $1^{st}$  left proleg of the larvae using the sterilised sewing pin and immediately after the PCL implant was inserted using sterilised tweezers. The larvae were placed into filter paper lined Petri dishes post insertion procedure and observed for 20 min. Larvae that showed excessive haemolymph loss or a protruding implant were euthanised by placing them into the  $-20^{\circ}$ C incubator for 20 min. After that, the larvae that tolerated the procedure well were placed into new filter paper lined Petri dishes allowing 10 larvae per plate. An injection of  $10\,\mu\text{L}$  of  $10^{-6}$  dilution of the bacterial culture and  $10\,\mu\text{L}$  of sterile PBS in the control groups was then injected into the top right proleg of the larvae. Post injection, the larvae were placed at  $37^{\circ}$ C and the mortality was observed for 24 h. The mortality was recorded upon the complete loss of larval movement.

#### Liquid chromatography-mass spectrometry (LC-MS/MS) analysis of biofilm

A quantitative and targeted tandem mass spectrometry method was developed for 6-hydroxyhexanoic acid (6OH-HA). The 6OH-HA ( $\sim$ 90% purity as a monomer) was purchased from Fisher Scientific (Loughborough, UK) and infused on a Sciex API5000 triple quadrupole mass analyser (Sciex, Framingham, MA, USA) coupled to an Agilent 1260 HPLC (Agilent, Loughborough, UK). Multiple reaction monitoring included three transitions at m/z 131.2 > 84.9 (quantifier), 131.2 > 87.0 (qualifier) and 131.2 > 113.0 (qualifier). Ionisation was achieved via electrospray ionisation (ESI) operated in negative polarity. The injection volume was 10  $\mu$ L and MeOH was used as a wash solvent between injections. A flow rate of 0.2 mL min<sup>-1</sup> was used for all analysis. Mobile phases A (0.1% acetic acid in H2O (v/v)) and B (0.1% acetic acid in MeCN(v/v)) were used for separation. The stationary phase was a Raptor biphenyl column,  $100 \times 2.1$  mm, 2.7  $\mu$ m particle size (Thames Restek, Saunderton, UK). All solvents used were of HPLC or LC-MS grade. The gradient profile was as follows: starting 10% mobile phase B; a linear ramp from 10 to 100% from 0.0 to 8.0 min; and holding at 100% B for a further 2.0 min before returning to the initial conditions, with a re-equilibration time of 5.0 min. There was a further needle wash and sample injection cycle time of 30 s, leading to a total run time of 15.5 min per sample.

Samples were prepared as described in the biofilm assay section except at the point of staining with crystal violet, the wells were instead filled with 200  $\mu$ L dH<sub>2</sub>O and the plate subsequently sonicated for 3 min to removed attached biofilms. For supernatant samples, the media was taken from the wells after incubation as part of the Biofilm Assay. Samples were filtered through a 0.2  $\mu$ M PVDF microcentrifuge filter (Fisher Scientific) centrifuged at 8,000 RPM for 2 min. The supernatant was transferred to a SureSTART amber glass Level 3 vial (Fisher Scientific) and subsequently injected onto the LC-MS/MS system. Quantifications were performed using calibration curves prepared in either ultra-pure water (specific resistance of 18.2 M $\Omega$  cm) or LB broth (i.e., matrix matched) with the 6OH-HA standard spiked at concentrations of 10, 25, 50, 100, 500 and 1000 ng/mL. Quantifications were conducted when linearity was acceptable, defined as R<sup>2</sup>  $\geq$  0.99.

#### **QUANTIFICATION AND STATISTICAL ANALYSIS**

Statistical analysis and graph construction was performed in Prism (version 10.0.3) throughout. Specific details of each test performed can be found in the relevant figure legend. Normality of data was assessed with a Shapiro-Wilk test in Prism. An alpha of 0.05 was used throughout, \* is p < 0.05, \*\* is p < 0.01, \*\*\* is p < 0.001, \*\*\*\* is p < 0.0001. Multiple comparisons were corrected with Dunnett's test, and adjusted p value presented. No data was excluded.